Nitrogen and carbon cycle perturbations through the Cenomanian-Turonian oceanic anoxic event 2 (94 Ma) in the Vocontian Basin (SE France)

Julien Danzelle, Laurent Riquier, François Baudin, Christophe Thomazo, Emmanuelle Pucéat

Nitrogen and carbon cycle perturbations through the Cenomanian-Turonian Oceanic Anoxic Event 2 (~94 Ma) in the Vocontian Basin (SE France)

Julien Danzelle [a*], Laurent Riquier [a], François Baudin [a], Christophe Thomazo [b], Emmanuelle Pucéat [b]

[a] Sorbonne Université, CNRS, UMR 7193 ISTeP, 4 Place Jussieu, 75005 Paris, France

[b] Université Bourgogne Franche-Comté, CNRS, UMR 6282 Biogéosciences, 6 Bd Gabriel, 21000 Dijon, France

*Corresponding author: julien.danzelle@sorbonne-universite.fr

Abstract

Oceanic Anoxic Event 2, spanning the Cenomanian-Turonian boundary, was an episode of major perturbations in global biogeochemical cycles, characterized by the widespread burial of organic carbon in both oceans and epicontinental basins. In the Vocontian Basin (SE France), this event was expressed by the deposition of the Niveau Thomel, a succession of interbedded dark shales, grey marls and bioturbated carbonates as observed in the Lambruisse section. Analyses of the total organic carbon (TOC) content, combined with the concentrations of redox-sensitive trace elements, revealed that conditions fluctuated from oxic to suboxic-anoxic during the deposition of the Niveau Thomel. Transient periods of deoxygenation were related to perturbations in nutrient cycling reflected by near-zero to negative $\delta^{15}N$ signatures indicative of increased diazotrophy.

The development of deoxygenated conditions in the Vocontian Basin was likely preconditioned by hydrographically restricted conditions, as confirmed by Mo vs. U enrichments, reducing bottom-water ventilation associated with water-column stratification. Intervals of reoxygenation were likely linked to climate-induced changes. In particular, a phase of regional or global cooling associated with a drop in pCO_2, called the Plenus Cold Event (PCE) resulted in vigorous reoxygenation of the Vocontian Basin.

Keywords: OAE 2; Anoxia; Redox; Trace elements; Nitrogen isotopes

1. Introduction

Several major perturbations of the global carbon cycle have been recognized. These episodes, namely oceanic anoxic events (OAEs; Schlanger and Jenkyns, 1976), are characterized by a widespread increase in organic matter (OM) content in the sedimentary record. The simultaneous deposition of organic-rich sediments in both epicontinental and deep-sea sites has been attributed to enhanced primary productivity in surface waters and/or to widespread oxygen-deficient conditions in bottom waters (see Arthur and Sageman, 1994; Jenkyns, 2010).

Oceanic Anoxic Event 2 (OAE 2), spanning the Cenomanian-Turonian boundary (CTB; 93.9 Ma) has been described as the most intense and widespread OAE of the Cretaceous (e.g. Jenkyns,

2010). The consequence of this episode of massive burial of ^{13}C-depleted OM was a worldwide positive excursion (+2 to 4‰) in the $\delta^{13}C$ signals of both carbonates and OM (Arthur et al., 1988; Jenkyns et al., 1994; Kuypers et al., 2002; Tsikos et al., 2004; Erbacher et al., 2005; Sageman et al., 2006; Jarvis et al., 2011). The interval encompassing this carbon isotope excursion used a chemostratigraphic signature of OAE 2 (Kuypers et al., 2002), is thought to have lasted between 450 and 700 kyr (Sageman et al., 2006; Voigt et al., 2008; Meyers et al., 2012; Eldrett et al., 2015).

The mechanisms involved in the development of favourable conditions for OM accumulation during OAE 2 are multiple and include an increase in primary productivity and OM export to depths, associated with an expansion of the oxygen minimum zone and a more sluggish ocean circulation (e.g. Schlanger and Jenkyns, 1986; Monteiro et al., 2012; Donnadieu et al., 2016).

Moreover, intense volcanic activity associated with the emplacement of large igneous province(s) (LIPs) is thought to triggered OAEs (Sinton and Duncan, 1997; Jones and Jenkyns, 2001). Ages reported for the Caribbean LIP (CLIP) (around 93–94 Ma; Snow et al., 2005) and for the High-Arctic LIP (HALIP) (Cenomanian–Turonian age; Tegner et al., 2011; Kingsbury et al., 2017), spanning the interval of OAE 2, support this inference. In addition, the isotopic compositions of hydrothermally-derived metals such as Os (Turgeon and Creaser, 2008; Du Vivier et al., 2014, 2015), Nd (MacLeod et al., 2008. Zheng et al., 2013) and Cr (Holmden et al., 2016), and geographically restricted enrichments of Hg (Scaife et al., 2017; Percival et al., 2018), point to intense submarine volcanic activity at the onset of OAE 2. A first consequence of this increased igneous activity was the emission of large amounts of CO_2 to the atmosphere-ocean system (e.g. Sinninghe Damsté et al., 2008; Barclay et al., 2010; van Bentum et al., 2012a). Higher sea-surface temperatures and a reduced latitudinal thermal gradient in the already extreme warm Cenomanian–Turonian climate (Clarke and Jenkyns, 1999; Pucéat et al., 2003; Bice et al., 2006; Forster et al., 2007; Friedrich et al., 2012; O'Brien et al., 2017) may have further limited oxygen solubility in surface waters and favoured more sluggish oceanic circulation.

The warm temperature and possibly accelerated hydrological cycle were associated with enhanced continental weathering and runoff (Blättler et al., 2011; Pogge von Strandmann et al., 2013; van Helmond et al., 2015), which may have increased nutrient input into the photic zone sustaining higher primary productivity. Enhanced freshwater input and higher runoff may also have triggered stratification of the water column and favoured oxygen-depletion in bottom waters in epicontinental settings, at least seasonally (van Helmond et al., 2015).

A second consequence of LIP emplacement was increased concentrations of hydrothermal iron and others trace metal micro-nutrients (Snow et al., 2005; Owens et al., 2012), which could have further enhanced primary productivity if associated with the development of upwelling, as simulated by some models (Trabucho Alexandre et al., 2010). Inputs of iron and trace metals into the photic zone as the result of such processes would have promoted nitrogen fixation by cyanobacteria (e.g. Kuypers et al., 2004) together with phosphorus released (linked to OM remineralization and instability of Fe-

Mn-oxyhydroxides) in stratified waters (Mort et al., 2007; Tsandev and Slomp, 2009; Kraal et al., 2010; Poulton et al., 2015; Beil et al., 2019). In addition, oxidation of the reduced metals and sulfides could have further to reduced free-oxygen concentration.

The overall anoxic water associated with OAE 2 were however interrupted by a reoxygenation event, as indicated by repopulation of benthic fauna (Kuhnt et al., 2004; Friedrich et al., 2006; Eldrett et al., 2014; van Helmond et al., 2016), a decrease in OM content, and changes in the concentrations of redox-sensitive element observed in sediments (Hetzel et al., 2011; van Helmond et al., 2014a; Dickson et al., 2016; Jenkyns et al., 2017; Danzelle et al., 2018). This event was contemporaneous with a southern input of boreal waters as testimony by boreal marine fauna in the Northern Hemisphere (Jefferies, 1962; Gale and Christensen, 1986; Kuhnt et al., 1986; Pearce et al., 2009; Eldrett et al., 2014; van Helmond et al., 2014b) and Nd isotopes (Zheng et al., 2013, 2016). This event is referred to as the Plenus Cold Event (PCE; Gale and Christensen, 1986) and was identified at several European and Atlantic sites. It has been argued to reflect a decrease in pCO_2 resulting from massive burial of organic carbon in sediments (Sinninghe Damsté et al., 2010; Jarvis et al., 2011).

In the Vocontian Basin (SE France), different phases of suboxic to anoxic conditions in bottom waters have been recognized on the basis of congruent sedimentary enrichment in OM, which is partially sulfurized (Raven et al., 2018; 2019), in varying iron sulfide concentrations, and in enrichments in redox-sensitive trace-element (e.g. Mo, V, Zn; Danzelle et al., 2018). Local bottom-water deoxygenation has been attributed to water column stratification forced by an upward migration of sulfide-rich conditions from the sediments, at least up to the sediment-water interface. Anoxic conditions could have further promoted deoxygenation by enhancing phosphorus recycling, leading to a positive feedback loop between primary productivity in surface waters and deoxygenation in bottom waters (Danzelle et al., 2018).

Expansion of sulfidic conditions in the Vocontian Basin could have been driven by an increase in sulfate and CO_2 availability in the oceans, possibly linked to the pulses of volcanic activity at the onset of OAE 2 (Adams et al., 2010). Oxygenation conditions during OAE 2 in the basin were unstable, as highlighted by variations in OM concentrations over time (Crumière, 1989; Jarvis et al., 2011; Danzelle et al., 2018). The contribution of other processes such as local/regional variations in primary productivity or in the hydrological cycle however remains poorly constrained.

In this study, we investigated the interaction between the intensity in deoxygenated conditions and variations in nutrient cycles by comparing changes in redox-sensitive elements with the carbon and nitrogen cycles for the Lambruisse section. We also compare fluctuations of oxygenation with climate to investigate the links between these processes, building on previous studies conducted in both epicontinental (e.g. Voigt et al., 2008) and deep-ocean environments (e.g. Dickson et al., 2016).

2. Geological setting

2.1. The Vocontian Basin through the CTB

The Vocontian Basin was part of the northern continental margin of the Alpine realm of the NW Tethys Ocean and was located at ~30°N (Philip et al., 1993). A north-south compressive regime developed in the Late Cretaceous, which was responsible for a high rate of subsidence in the deeper and eastern parts of the basin (Porthault, 1974; Grosheny et al., 2017), with a recently proposed tectonic pulse around the CTB (Grosheny et al., 2017). This tectonic context provided space for the gradual filling of the basin, dominated by a thick rhythmically bedded hemipelagic limestone–marl succession. The paleodepth at the centre of the Vocontian Basin during CTB times is estimated to have been a few hundred metres (Grosheny et al., 2006).

In the deepest part of the basin, a distinctive change in facies through the CTB interval is characterized by a ~20–25 m interval composed of alternating dark organic-rich calcareous shale and limestone (Crumière, 1989; Grosheny et al., 2006; Takashima et al., 2009; Jarvis et al., 2011). This interval, named the Niveau Thomel, is the local sedimentary expression of OAE 2 recording the globally recognized carbon isotope positive excursion (Morel, 1998; Takashima et al., 2009; Jarvis et al., 2011; Gale et al., 2019).

2.2 The Lambruisse section

The Lambruisse section (44°02'05N; 06°28'00E) is one of the tectonically unaffected successions of the deep eastern part of the Vocontian Basin (Fig. 1A), exposing the Niveau Thomel. Based on lithology, four units can be distinguished within the Niveau Thomel, called TH1 to TH4 from the base to the top, following the description Jarvis et al. (2011) used for the Pont d'Issole section (Fig. 2). The following description of the faunal content along the Lambruisse section is from Takashima et al. (2009).

The base of the section (~17 m) preceding the Niveau Thomel is formed by an alternation of highly bioturbated white and light grey limestones and grey marls. This pre-Thomel unit yields abundant planktonic foraminifera. An interval at the base of the Niveau Thomel, estimated to be 4 m thick, was unfavourable for lithological description or sampling. This interval corresponds to the major part of TH1. The estimated thickness of TH1 (4 m of hidden and uppermost 1 m of exposed dark shales) is in agreement with the 4.5–5 m thick TH1 described in Pont d'Issole section located at a distance of ~4 km (Jarvis et al., 2011; Danzelle et al., 2018). These dark shales are devoid of benthic foraminifera.

Unit TH2 (4.2 m) corresponds to a return to alternating light grey marly limestones and grey limy marls, both highly bioturbated. This unit contains abundant planktonic and benthic foraminifera, sponge spicules and radiolarians.

Unit TH3 (5.8 m) is composed of alternating dark laminated and non-bioturbated calcareous shales and sparsely-bioturbated grey limy marls. Unlike the dark shales, the limy marls contain some dwarf planktonic foraminifera, abundant radiolarians and sponge spicules.

Unit TH4 (7.2 m) is composed of alternating of moderately to highly bioturbated limestones with dark shale and moderately bioturbated marls rich in radiolarians, planktonic and benthic foraminifera. The top of TH4, and therefore of the Niveau Thomel, was placed at the top of the last dark shale bed.

The top of the section (~14 m) is dominated by thick white highly-bioturbated limestone beds rich in radiolarians, planktonic and benthic foraminifera. This interval also contains thin grey marl intercalations and one 60 cm dark calcareous shale interbed, ~8.5 m above the top of the Niveau Thomel.

3. Methods

A total of 91 samples were analyzed in this work. The approach included the analysis of sedimentary OM by Rock-Eval analysis, carbonate carbon and oxygen isotope composition, organic carbon and bulk nitrogen isotope composition, and of concentrations of major- and trace-elements of bulk rock. Bulk-rock samples were powdered to ~10 μm using a ring and puck mill at Sorbonne University's ISTeP laboratory.

3.1. Rock-Eval pyrolysis

Following sequential pyrolysis and oxidation treatment (Espitalié et al., 1985a, b, 1986; Behar et al., 2001) of 60 mg aliquots of powdered bulk sample, total organic carbon content (TOC wt%), Hydrogen Index (HI) and Oxygen Index (OI) in samples were determined with a Rock-Eval™ 6 at the Sorbonne University's ISTeP laboratory of. Based on duplicates of the IFPEN 160000 standard, reproducibility (1σ) was estimated at ± 0.05 wt% for TOC, ± 10 mg HC/g TOC for HI and ± 10 mg CO_2/g TOC for OI. As HI and OI values are not reliable when TOC < 0.4 wt% (Espitalié et al., 1986; Peters, 1986), the HI and OI presented in this paper are only reported for samples containing at least 0.4 wt% TOC.

3.2. Carbon and oxygen isotope compositions of carbonate

The stable carbon ($\delta^{13}C_{carb}$) and oxygen ($\delta^{18}O$) isotope compositions of carbonates were determined in 50 powdered bulk-rock samples. Depending on the sample carbonate content, 60 to 200 μg aliquots were loaded in glass vials with 100% H_3PO_4 at 70°C. Carbon and oxygen isotopic compositions were measured on a Thermo Scientific™ Delta V™ IRMS coupled with a Kiel VI

carbonate preparation device at the Biogeosciences Laboratory of the Bourgogne-Franche-Comté University. All isotopic values are reported in the standard δ-notation (permil ‰) relative to V-PDB (Vienna Pee Dee Belemnite) by calibration to $\delta^{13}C$ value of +1.95‰, and $\delta^{18}O$ value of -2.20‰ of the NBS19 international standard. External reproducibility was checked by replicate analyses of both NBS19 and in-house laboratory standards and was better than ±0.08 ‰ for $\delta^{18}O$ and ±0.04 ‰ for $\delta^{13}C$ (1σ).

3.3. Carbon isotope composition of organic matter

The stable carbon isotope composition of OM ($\delta^{13}C_{org}$) was determined on carbonate-free residues collected from 83 samples at the Biogeosciences Laboratory. Decarbonation was carried out by placing powdered samples in reaction tubes filled with 25 ml of 6N HCl solution for 12 hours at room temperature. The dried residues were weighed (between 30 and 75 mg based on Rock-Eval results) and poured into tin capsules. The capsules were combusted using a Vario MICRO cube elemental analyser (Elementar GmbH™) at 950°C coupled with an IsoPrime stable-isotope mass spectrometer (IsoPrime, Manchester, UK). The isotopic results are reported in δ-notation relative to the V-PDB and calibrated using USGS40 certified reference L-glutamic acid ($\delta^{13}C_{org}$ = -26.2‰, TOC = 40.82 wt%). Reproducibility (1σ) was better than ± 0.10 ‰ for $\delta^{13}C$, ± 0.10 wt% for C_{org} concentration, based on replicated samples.

3.4. Nitrogen isotope composition of bulk rock

Stable nitrogen isotope compositions ($\delta^{15}N$) of the carbonate-free samples were determined on the same 83 samples run in parallel to the $\delta^{13}C_{org}$ analyses using the same apparatus. The isotope compositions are reported in δ-notation relative to AIR and calibrated using USGS40 certified reference values ($\delta^{15}N$ = -4.5‰, TN = 9.52 wt%). Reproducibility (1σ) was better than ± 0.30‰ for $\delta^{15}N$, ± 0.02 wt% for N concentration, based on replicated samples.

3.5. Concentrations of major and trace-element

Concentrations of major (Al, Fe, Mn) and trace-elements (Mo, U, V, Zn) of 90 selected samples were determined respectively with an ICP-OES (Thermo Fisher iCap 6500) and an ICP-MS (7700X Agilent) at the spectrochemical laboratory of the Service d'Analyse des Roches et des Minéraux of the Centre National de la Recherche Scientifique (Vandoeuvre-les-Nancy, France). Sample preparation consisted in a fusion by $LiBO_2$ followed by acid digestion by HNO_3 (2%) (Carignan et al., 2001). Analyses of international standards and replicate samples indicated levels of accuracy and precision better than 1% for Al, Fe, Mn; 5% for Ba; 10% for Cu, Mo, Ni, Zn and 15% for Co and U.

To distinguish major and trace elements of detrital origin from those representative of the marine background, concentrations were normalized to Al (cf. Calvert and Pedersen, 1993; Morford et al., 2001). Aluminium is a robust tracer of detrital input and it is not involved in or affected by biological or diagenetic processes. In this study, element/Al (X/Al) ratios are expressed in terms of enrichment factors (EF). This representation corresponds to the ratio between the X/Al values in the sample and that in a reference, in this case average Upper Continental Crust (UCC) (Taylor and McLennan, 1995; McLennan, 2001), and is expressed as EF X = $(X/Al)_{sample}/(X/Al)_{UCC}$. The purpose of EF values is to easily quantify the enrichment (EF > 1) or depletion (EF < 1) of an element compared to its detrital value (EF = 1).

4. Results

4.1. Organic content

As expected, the variation in organic content throughout the section is in accordance with changes in facies, with dark intervals corresponding to the highest TOC values. TOC measurements, obtained by Rock-Eval in this study (Fig. 2), resemble to those obtained using an elemental analyser by Takashima et al. (2009).

In the pre-Thomel interval, mainly dominated by limestone beds, TOC never exceed 0.50 wt%. The organic content of the upper part of the TH1 is characterized by dm-scale fluctuations between 0.25 wt% and 2.45 wt%. Unit TH2 represents an abrupt fall in the organic content (TOC mostly lower than 0.30 wt%). One very thin organic-rich marl interbed (TOC = 1.50 wt%) is present just before the TH2–TH3 boundary. In TH3, high frequency oscillations occurred between lower TOC values (0.20 < TOC < 0.75 wt%) in the grey marls and higher TOC values (1.25 < TOC < 3.10 wt%) in the dark shales. Unit TH4 marks a progressive return to low organic content (TOC < 0.35 wt%); two dark shale beds observed at 36.50 m and at 39.60 m in this unit contain respectively 1.40 and 0.90 wt% TOC. Finally, two marly levels at the base and at the top of the post-Thomel dark calcareous shale bed presents TOC values of 1.30 wt% (at 48.00 m) and 0.80 wt% (at 49.56 m) respectively.

4.2. Stable carbon isotopes

The stable carbon isotope composition of carbonates in the Lambruisse section, previously documented by Takashima et al. (2009), were redetermined here to evaluate the differences between the isotopic compositions of coexisting carbonate and organic carbon in order to investigate changes in of the $\Delta^{13}C$ (defined as $\Delta^{13}C = \delta^{13}C_{carb} - \delta^{13}C_{org}$) signal, as reported for the equivalent succession at Pont d'Issole by Jarvis et al. (2011).

4.2.1. Carbonate stable carbon isotopes

The $\delta^{13}C_{carb}$ signal obtained in this work (Fig. 2) is consistent with that reported by Takashima et al. (2009). In the pre-Thomel interval, $\delta^{13}C_{carb}$ remained relatively stable and only fluctuated slightly around a mean of 2.38 ± 0.08‰ (1σ). As the lower part of TH1 was not exposed, the base of the first build-up phase of the positive isotope excursion characterizing the onset of OAE 2 (Jarvis et al., 2006, 2011) could not be determined here. The $\delta^{13}C_{carb}$ curve presented by Takashima et al. (2009), highlighted a +0.70‰ shift exactly at the base of the Niveau Thomel, confirming the temporal link between the change in facies in the Vocontian Basin and the onset of OAE 2.

A major increase in $\delta^{13}C_{carb}$ is recorded from the top of TH1 to the middle of TH2 (from 2.8 to 4.0‰) which represents an acceleration in the positive excursion, also documented at Pont d'Issole (Jarvis et al., 2011). The maximum value recorded in TH2 thus corresponds to peak "A" described by Jarvis et al. (2006) in the Eastbourne section (England). The upper half of TH2 is marked by a trough in the positive excursion, with $\delta^{13}C_{carb}$ values oscillating between 3.5 and 3.7‰ prior to a second increase recorded at the TH2–TH3 boundary toward peak "B" ($\delta^{13}C_{carb}$ = 4.5‰). An interval of relatively constant and high $\delta^{13}C_{carb}$ values, termed the isotopic "plateau" (Paul et al., 1999), corresponds to Unit TH3 and to the base of Unit TH4 (mean $\delta^{13}C_{carb}$ = 4.24‰). The total amplitude of the $\delta^{13}C_{carb}$ positive excursion, from pre-Thomel values to the maximum values recorded in TH3, thus reached about 2‰. The highest $\delta^{13}C_{carb}$ value corresponds to the peak "C" (4.5‰) and is located right before the termination of OAE 2, which is underlined by a last small positive peak in the decreasing phase. Based on the chemostratigraphic correlation with the $\delta^{13}C$ signals from the Eastbourne (Paul et al., 1999) and Pueblo (Kennedy et al., 2005) sections, where the CTB was defined as the limit between the *Neocardioceras judii* and *Watinoceras devonense* ammonite biozones, the CTB at Lambruisse was placed in the small trough before peak "C", at 31.60 m. Unit TH4 marks a return to lower $\delta^{13}C_{carb}$ values that follows the positive excursion. However, two small positive peaks (~+0.4‰) can be observed in this more stable interval of lower $\delta^{13}C_{carb}$ values, and correspond to two organic-rich interbeds. The slight decrease in $\delta^{13}C_{carb}$ above the Niveau Thomel is interrupted at the top of the section by a small (~0.4‰) positive excursion in the vicinity of the last organic-rich interbed.

4.2.2. Stable carbon isotopes of organic matter

Changes in the carbon isotope composition of OM through the Lambruisse section resemble to those of carbonate (Fig. 2). Higher resolution sampling (supplementary data) made it possible to identify the transitions between the different phases depicted in the carbon isotope chemostratigraphic signal more precisely. Below the Niveau Thomel, $\delta^{13}C_{org}$ values oscillate between -26.8 and -25.7‰ towards the onset of OAE 2 (Fig. 2). In the upper part of TH1, $\delta^{13}C_{org}$ values are relatively low (-26.7‰ minimum), similar to the lowest pre-OAE 2 ones. A negative shift may be associated with Unit TH1, as described in the Pont d'Issole section (Jarvis et al., 2011). $\delta^{13}C_{org}$ rises sharply at the TH1–TH2 boundary, from -26.7‰ to a maximum of -24.3‰ at peak "A". This rise corresponds to the first

major step of the worldwide OAE 2 positive excursion. The trough in the positive excursion, between peaks "A" and "B" in the $\delta^{13}C_{org}$ profile, has an amplitude of 1.5‰ (from -25.5‰ for the lowest TH2 value to -24.0‰ for peak "B"). Within the "plateau" phase, the $\delta^{13}C_{org}$ profile shows several small peaks and troughs below 1.1‰ in amplitude and around a mean value of -24.7‰. The recovery phase after peak "C" (-24.3‰) is similar in terms of amplitude (-1.7‰) to that of the $\delta^{13}C_{carb}$ signal (-1.5‰) and is followed by positive +~0.8‰ peaks in TH4. The post-Thomel interval is first characterized by a negative shift (-1.7‰) from -25.3‰ at the top of TH4 to -27.0‰ located in the dark shale interval at 48.00 m, followed by a positive shift toward -25.4‰ (at 50.50 m).

4.2.3. Paired carbon isotope signal ($\Delta^{13}C$)

The $\Delta^{13}C$ signal shows quite strong variability in the pre-Thomel interval between 28.0 and 29.2‰, with a mean value of 28.8 (± 0.4‰, 1σ) (Fig. 2). The top of TH1 is characterized by higher values reaching 29.5‰ followed by a sharp negative shift at the base of TH2 with $\Delta^{13}C$ values decreasing to 27.6‰. The entire TH2 is characterized by relatively low $\Delta^{13}C$ value with a mean of 28.3 (± 0.4‰, 1σ). The upper limit of TH2 corresponds to a transition toward higher values in the entire TH3 Unit with a mean $\Delta^{13}C$ value of 29.1 (± 0.3‰, 1σ). The end of OAE 2 is marked by a negative shift toward 28.1‰ at the base of TH4, followed by a positive shift at the end of TH4 reaching 29.4‰. The post-Thomel is characterized by $\Delta^{13}C$ reaching 30.0 ‰ in the dark shale bed at 48.00 m.

4.3. Stable oxygen isotopes

Stable oxygen isotope compositions through the Lambruisse section display a long-term increase from the base of the section towards the base of TH3 (Fig. 2). Within this long-term trend, a first increase in $\delta^{18}O$ values, from values of about -4.0‰ to about -3.5‰ is recorded prior to OAE 2, approximately 5 m above the base of the section. Oxygen isotope compositions remain quite stable at around -3.5‰, up to the base of the Niveau Thomel. A progressive positive shift is then recorded from the upper TH1 ($\delta^{18}O$ = -3.5‰) towards the base of TH3 ($\delta^{18}O$ = -2.7‰), which yield the highest $\delta^{18}O$ values of the entire section. Beginning with this maximum and in units TH3 and TH4, $\delta^{18}O$ displays an overall negative trend with superimposed oscillations. This decreasing trend culminates at about 1.5 m above the top of the Niveau Thomel ($\delta^{18}O$ = -4.7‰) in the Turonian. The upper part of the section shows highly fluctuating $\delta^{18}O$ values, with a possible increasing trend of about ~+1.0‰.

4.4. Stable nitrogen isotopes, N concentrations and C/N molar ratios

First-order variations in $\delta^{15}N$ match the lithological units. The pre-Thomel unit presents variable positive $\delta^{15}N$ values of 1.5 ± 0.7‰, associated with relatively low N concentrations (0.09 ± 0.04 wt%, 1σ) and a relatively low carbonate-free C/N molar ratio (9.8 ± 3.2) (Fig. 3).

In the upper part of TH1, the $\delta^{15}N$ fluctuate considerably around a mean of 0.8 (± 0.9‰%, 1σ), to reach negative values of -0.3‰. This interval also corresponds to higher but fluctuating N sedimentary concentrations ranging from 0.08 to 0.21 wt% and higher C/N molar ratios varying ranging from 7.1 to 18.6. In TH2, the $\delta^{15}N$ profile first shifts towards more positive values from the TH1–TH2 transition towards the middle of the unit ($\delta^{15}N$ up to +2.5‰), and then decreases towards the top of TH2. Only one sample, located at +25.80 m in the only organic-rich level, shows a negative $\delta^{15}N$ value (-0.2‰). This sample also has a higher concentration of N (0.16 wt%) and a higher C/N ratio (17.14), than the rest of the unit (N = 0.08 ± 0.02%%, 1σ and C/N = 8.5 ± 2.4%, 1σ). Like TH1, TH3 and the base of TH4 are characterized by high-frequency oscillations in the $\delta^{15}N$ signal between +2.1 and -0.7‰, N concentrations fluctuating between 0.06 and 0.23%, and a C/N ratio fluctuating between 8.1 and 22.1. Finally, the top of TH4 is characterized by a return to more positive $\delta^{15}N$ values reaching +2.7‰, low N concentrations (< 0.10 wt%) and low C/N ratios (< 10). However, two organic-rich marly beds in this interval yield lower $\delta^{15}N$ values, disrupting the general increasing trend, with higher N concentrations, reaching 0.16 wt% in both cases. In those two intervals, C/N ratios reach 19.4 and 15.4, respectively. Finally, the last organic-rich bed, of Turonian age, at +48.00 m (with a TOC of 1.3 wt%) presents values ($\delta^{15}N$ = -0.8‰; N = 0.23%; C/N = 21.7) which are as extreme as those in TH1 or TH3.

4.5. Major and trace element geochemistry

To evaluate the abundances and the authigenic (or biogenic) nature of the major- and trace-elements measured through the Lambruisse section, the correlation coefficient (r-value) and associated probability (p-value) for each element against Al were determined (Table 1). High r-values (> 0.7) for U and V revealed that variations in these elements are highly influenced by the detrital content, with the exception of some limited values above the X/Al regression line indicating sporadic authigenic enrichments. Intermediate r-values obtained for Cu, Ni, Zn and TOC (r < 0.7) show they were influenced by both redox/productivity conditions and detrital supply. Conversely, Ba is poorly correlated with Al (r < 0.4) and fluctuations in the concentrations of these elements mainly reflect authigenic variation. Molybdenum is also poorly correlated with Al (r = 0.1), but all sample values (n = 23) correspond to TOC-rich levels. Phosphorus, a macronutrient for primary productivity, is not presented here because phosphorus concentrations in only two samples were significantly above the detection limit (i.e. 0.04%).

4.5.1. Redox-sensitive elements with minimal detrital influence

Molybdenum, vanadium and uranium are commonly considered to be robust proxies for the evaluation of redox conditions (e.g. Tribovillard et al., 2006). More specifically, reduced species of these elements have the ability to form insoluble chemical precipitate in presence of sulfides, and to form complex with OM. Variations in their enrichment factors (EF) broadly follow the TOC, resulting in distinct values recorded between the relatively enriched dark shales (TOC > 1.0 wt%) compared to the grey marl and carbonate intervals.

Measurable concentrations of Mo ([Mo] > 0.5 ppm) were only detected in the upper TH1, TH3, the base of TH4, and in the post-Thomel organic-rich bed (Fig. 4). Significant enrichments are observed in the dark shale packages of the TH3. The maximum Mo enrichment is recorded in the middle TH3 (EF Mo up to 8.5). Those EF Mo peaks alternate at the dm-scale with near Upper Crust values (EF ~1) or with samples showing depleted values.

Like Mo, V presented only limited and oscillating enrichments (EF V up to 4.7) in the Niveau Thomel and post-Thomel organic-rich bed. However, in contrast to Mo, maximum enrichment in V is observe at the base of TH4. Apart of these intermittent enrichments, the values for the large majority of the section are very close to those of the UCC.

Even more limited uranium enrichments are recorded here than in crustal detrital background. In the Niveau Thomel, EF U never exceeds 2.4 and the highest value is observed in the post-Thomel organic-rich bed (EF U = 4.0).

4.5.2. Redox-sensitive elements influenced by productivity

Copper, nickel and zinc are micronutrients (e.g. Calvert and Pedersen, 1993) and are consequently widely used as paleoproductivity proxies (e.g. Algeo and Maynard, 2004). Enrichment in Cu, Ni and Zn in sediments indicates, first, scavenging by OM and/or by Fe-Mn-oxyhydroxides. Reductive dissolution of these oxyhydroxides and OM decay in sediments may release Cu, Ni and Zn into pore waters. Under bacterial sulfate reducing conditions (sulfidic), they may coprecipitate with sulfides (e.g. Morse and Luther, 1999). Barium could also indicate of paleoproductivity because of its incorporation in phytoplankton. However, barite is unstable under sulfidic conditions and a diagenetic barite-front may be formed in the case of reoxygenation (e.g. McManus et al., 1998).

Zinc enrichments are scattered throughout the section. Background EF Zn values remain around 2.0 from the base of the section to the top of the Niveau Thomel but reach 4.0 at the top of the section. Within TH3, some intermittent enrichments are significant (EF up to 9.7) and stratigraphically synchronous with the highest EF V values. In contrast to Mo, V and U, some Zn-enriched samples are present below the Niveau Thomel (EF up to 6.1). Another difference from Mo, V and U chemostratigraphy is the presence of a peak of EF Zn in TH2.

Nickel enrichments are low and never exceed 2.5 in the organic-rich intervals of the Niveau Thomel. The highest EF Ni is recorded at the top of TH2 (EF = 3.8). Like for Zn, TH2 is marked by progressive enrichment in Ni. Most EF Ni values above the Niveau Thomel remain stable around 1.5 but a relatively higher value (EF = 3.2) is recorded in the organic-rich interbed at the top of the section.

Similarly, Cu is not specifically seen to be enriched in the organic-rich intervals, except in TH3 (EF up to 5.7). A small enrichment is again visible in TH2 (EF up to 4.4). The main feature of the EF Cu chemostratigraphy is a transition from near UCC background values (EF~1.2–2.7) in the interval from the base of the section to the top of TH3, toward elevated EF Cu in TH4 and in the post-Thomel deposits (3.2 < EF Cu < 6.7).

None or only scarce Ba enrichments are recorded in most of the section, except in two intervals. The first is in TH2 (EF up to 5.3) synchronous with enrichments in Zn, Ni and Cu. Another sharper peak occurs at the top of TH3 (EF up to 7.2) but is not associated with enrichments in TOC, Mo, V, U, Zn, Ni or Cu.

5. Discussion

5.1. Preservation of organic matter

5.1.1. Characterization of organic matter

Organic matter concentrations in Units TH1 and TH3, described as “black shale” intervals by Jarvis et al. (2011), are relatively modest compared to those recorded at sites on the southern margin of the Central Atlantic, where the TOC reaches exceptionally high values in the OAE 2 section (up to 56 wt% at DSDP Site 367; Dickson et al., 2016). In the Vocontian Basin, maximum TOC values recorded at Lambruisse (up to 3.1 wt%) resemble those at Pont d’Issole (3.5 wt%; Jarvis et al., 2011) but are higher than those at Clot Chevalier (1.5 wt%; Gale et al., 2019).

The other shared characteristic of these Vocontian sites is that TOC values fluctuate greatly at the scale of individual units but also within the organic-rich intervals, indicating that the conditions which favoured OM burial in the basin were highly unstable throughout OAE 2. This resembles the record in other epicontinental basins for example, the Briançonnais domain (Charbonnier et al., 2018), Lower Saxony Basin (Hetzel et al., 2011) and the Western Interior Basin (e.g. Eldrett et al., 2014) where similar TOC contents are recorded (up to 4.9, 2.5 and 5.6 wt%, respectively). Large variations in TOC content during OAE 2 were also observed in Central Atlantic or Italian sites were values respectively can reach 56 wt% and 26 wt% respectively (Tsikos et al., 2004; Scopelliti et al., 2008; Hetzel et al., 2009; Dickson et al., 2016). The TOC fluctuations result therein from a combination of global and local conditions (i.e. basin configuration and local primary productivity).

At Lambruisse, the origin of the OM was inferred by comparing HI and OI values in a modified Van Krevelen diagram (Fig. 5). Samples with high TOC values (TOC > 1.0 wt%) in the OAE 2 interval and in the Turonian dark shale beds present HI and OI values typical of Type II OM, indicating that organic-rich intervals reflect marine primary production. The trend from the Type II toward Type III poles in Fig. 5 suggests either OM oxidation or increased influence of terrestrial OM. The two processes are not incompatible as the samples assigned to Type III had the lowest organic content.

Analysis of the palynomorphs along the Pont d'Issole section by Jarvis et al. (2011) showed that the low TOC intervals are associated with a high (> 0.7) proportion of marine to terrestrial palynomorphs. Considering a preferential degradation of labile marine over terrestrial OM under well-oxygenated conditions, intervals in which low TOC and HI values were measured are presumably associated with a largely dominant marine OM downward flux. This inference is in accordance with oxidized OM in low TOC intervals rather than a large proportion of terrestrial OM.

5.1.2. Redox conditions and basin configuration

The combination of enrichments in several elements that are highly sensitive to reduced conditions (Mo, U, V) is an efficient tool for reconstructing redox conditions in the past (Algeo and Maynard, 2004; Brumsack, 2006; Riquier et al., 2006; Tribovillard et al., 2006; Westermann et al., 2014). Significant enrichment factors (EF > 3; cf. Algeo and Tribovillard, 2009) were only observed with elevated TOC (> 1.0 wt%) (Fig. 4) similarly to Pont d'Issole (Danzelle et al., 2018), confirming that higher OM concentrations are associated with better preservation conditions caused by depleted oxygen concentrations, or that a higher flux of sedimentary OM caused oxygen depletion at Lambruisse. What is more, the maximum enrichments measured (EF Mo = 8.5; EF V = 4.7; EF U = 2.1) are only moderate compared to the extremely organic-rich sections in the Central Atlantic or Western Tethys, where EF often exceed 100 for Mo and 10 for V and U (e.g. Brumsack, 2006; Hetzel et al., 2009, Westermann et al., 2014).

As observed at Pont d'Issole (Danzelle et al., 2018), Mo had higher enrichment factors than V and U during OAE 2. During typical gradual oxygen depletion, U and V, reduced under denitrifying conditions, can accumulate before Mo, which is enriched under sulfidic conditions (e.g. Tribovillard et al., 2006). At Pont d'Issole, trace metal enrichments and degree of pyritization (DOP) data correlated with TOC values revealed that the bottom waters oscillated between suboxic and anoxic conditions in the organic-rich intervals (Danzelle et al., 2018). Similar enrichment factors at Lambruisse suggest that higher enrichments are related to anoxic conditions in bottom waters. Tribovillard et al. (2004a) demonstrated that the sulfurization of marine OM in sediments can preferentially capture Mo over time. The highest peaks in Mo observed in TH1 and TH3 at Lambruisse correlated with intervals with

high DOP (Danzelle et al., 2018) and S/C values in the organic fraction characterizing the highly sulfurized OM described at Pont d'Issole (Raven et al., 2018, 2019).

Molybdenum and uranium have not only been extensively studied to evaluate redox conditions but also to reconstruct hydrographic conditions in the past (Algeo and Tribovillard, 2009; Algeo and Rowe, 2012; Tribovillard et al., 2012; Westermann et al., 2014; Dickson et al., 2016, 2017). Because of the different geochemical behaviour of Mo and U under anoxic conditions, the covariation between their respective enrichments in sediments has been considered as a tool to evaluate the geometry of a basin (Algeo and Tribovillard, 2009; Tribovillard et al., 2012). Uptake of authigenic U in sediments is effective under suboxic conditions at the Fe(II)-Fe(III) redox boundary, while Mo only accumulates in sediments in the presence of free H_2S (sulfidic conditions). In an environment characterized by gradual oxygen depletion, U is thus enriched in sediments before Mo. As Mo readily accumulates when sulfidic conditions are encountered in the sediments and in the water column, the EF Mo vs. EF U trend from oxic to euxinic conditions displays a concave upward profile (Fig. 6). This trend only applies to non-limited Mo and U contents, in open marine environments. Under restricted conditions, characterized by a redox stratified water column, Mn and Fe oxyhydroxides formed in the upper oxic part of the water column, which are unstable under sulfidic conditions, are partially recycled back into the water column in their reduced soluble forms (Van Cappellen et al., 1998; Dellwig et al., 2010). Recycling affects Mo behaviour in particular because it can be scavenged by Mn-oxyhydroxides resulting in its transport from the water column to the sediments (Algeo and Tribovillard, 2009; Dellwig et al., 2010). This process is called "particulate shuttle" effect (Fig. 6). In the case of sulfidic conditions in sediments or in the lower part of the water column, the Mo transported by the Mn-oxyhydroxides is delivered to the sulfidic zone and is fixed by sulfidation. Reduced Mn can diffuse back to the oxic part of the water column and reform oxyhydroxides, repeating the process and leading to a larger quantity of Mo fixed in sediments than U (Crusius et al., 1996).

The majority of the samples at Lambruisse presented higher Mo than U enrichments and are located along a vector towards the particulate shuttle zone (Fig. 6), i.e., the most TOC enriched samples are located farthest from the unrestricted marine trend. We therefore argue that the Vocontian Basin was probably, at least weakly restricted, and that a deep chemocline at the sediment-water interface episodically expanded into bottom waters, triggering a Mn cycle in the water column, as proposed for Pont d'Issole (Danzelle et al., 2018). This interpretation is in agreement with the results of a recent study by Grosheny et al. (2017). These authors propose that the Vocontian Basin was affected by a short-lived compressive tectonic pulse at the CTB, leading to confinement of the basin at that time.

5.1.3. Productivity conditions

514 The relationship between the enrichments in elements associated with primary productivity
515 and OM content is somewhat erratic. First, most of the enrichments during OAE 2 are low compared
516 to those in the southern Central Atlantic and Western Tethys sites (Brumsack, 2006) suggesting
517 moderate primary productivity at Lambruisse. During the carbon isotope plateau, only four near
518 concomitant peaks of Zn and Ni (EF Zn > 4; EF Ni > 2) are visible (Fig. 4). These peaks, which
519 coincide with the highest enrichments in V and U (Fig. 4), suggest a higher organic flux associated
520 with enhanced preservation due to the formation of sulfides (Tribovillard et al., 2006).
521 In contrast to Ni, Cu does not covary with TOC even though these two elements generally
522 display similar geochemical behaviour (Tribovillard et al., 2004b). The distinctive behaviour of Cu
523 can be attributed to its capacity to be scavenged from solution in deep water (Boyle et al., 1977). The
524 increasing trend of EF Cu through the carbon isotope plateau interval with the highest values observed
525 after the termination of OAE 2 (Fig. 4) could represent a deepening of the bottom water associated
526 with the end of the OAE 2 sea-level rise, rather than a long-term increase in primary productivity.
527 Enrichments in barium are low (EF Ba dominantly < 3) even in organic-rich intervals (Fig. 4),
528 in stark contrasts with EF Ba > 50 observed in the Bonarelli level in Tethyan domain, which was
529 interpreted as representing high primary productivity (Turgeon and Brumsack, 2006), and confirms
530 that the Vocontian Basin did not experience intense eutrophication of the surface waters. The single
531 Ba peak in the carbon isotope plateau interval was found in a carbonate interbed overlying a dark shale
532 interval with the highest TOC value in the succession. This peak likely represents the diagenetic
533 formation of barite ($BaSO_4$) either under the form of a front or of nodules (McManus et al., 1998).
534 This suggests that the oxygenation front, and the dissolved sulfate, may have migrated downwards in
535 the sediments, inducing precipitation of the dissolved Ba accumulated in the pore waters. This
536 interpretation is coherent with a reoxygenation following the interval presenting the highest TOC and
537 EF Mo values of the Niveau Thomel indicating more intense sulfate-reducing conditions within the
538 sediments, confirming the difficulty to employ Ba as a paleoproductivity proxy.
539 In contrast to the rest of the OAE 2 interval, the PCE is a phase of relative enrichment in Ni,
540 Cu, Ba and to a lesser degree in Zn, culminating in the only organic-rich bed of PCE at +25.80 m
541 (TOC = 1.48 wt%), probably the result of a short-lived increase in primary productivity. Jenkyns et al.
542 (2017) and Sweere et al. (2018) proposed that those elements contained in sulfides and/or in organic
543 matter, were released due to increasing aerobic biodegradation during the PCE. Moreover, enhanced
544 mixing of the entire water column could have promoted the recycling of these elements from bottom
545 waters towards the surface waters, favouring continued primary productivity throughout OAE 2
546 (Forster et al., 2007; Parente et al., 2008).
547

548 **5.2. Perturbation of the nitrogen cycle**
549

The chemostatigraphy of the nitrogen isotope signal revealed occurrences of negative $\delta^{15}N$ excursions in the organic-rich intervals, in OAE 2 (towards -0.7‰) and in the post-OAE 2 interval (towards -0.8‰) (Fig. 3). This relationship is clearly displayed by a $\delta^{15}N$ vs. TOC crossplot (Fig. 7A). As the HI parameter is positively correlated with TOC (Fig. 5), given a predominantly marine-origin for the OM, the relationship between $\delta^{15}N$ and HI (Fig. 7B) indicates that sedimentary $\delta^{15}N$ variations are not influenced by a changing contribution of continental OM and, therefore, reflect changes in the oceanic biogeochemical N cycle.

Nitrogen isotope compositions of sediments was widely used as as an indicator of nitrogen biogeochemistry and for the reconstruction of redox conditions in the past (e.g. Ader et al., 2014, 2016; Algeo et al., 2014) and particularly during OAE 2 (Kuypers et al., 2004; Arnaboldi and Meyers, 2007; Ohkouchi et al., 2006; Jenkyns et al., 2007; Junium and Arthur, 2007; Blumenberg and Wiese, 2012; Higgins et al., 2012; Algeo et al., 2014; Ruvalcaba Baroni et al., 2015; Zhang et al., 2019). The nitrogen cycle is dominated by biologically induced mechanisms that depend on the oxygenation state of the water column and of the sediments. Transitions between the oxidized and reduced forms of N are associated with isotopic fractionation (e.g. Thomazo et al., 2011). Under oxygenated conditions in the water column, ammonium (NH_4^+) released by remineralized OM is oxidized to nitrite (NO_2^-) and nitrate (NO_3^-) through nitrification processes, and can be assimilated by photosynthetic organisms. Dentrifying bacterial using the NO_3^- for oxidizing the OM, particularly within the oxygen-minimum zone, involves a large fractionation that results in a ^{15}N-enriched residual reservoir of NO_3^- as observed in present-day oceans with ~+7‰ average isotopic composition (Tesdal et al., 2013), which is in agreement with the ~5‰ average composition of NO_3^- in the oceans (Sigman et al., 2005).

Under oxygen-depleted environments, NH_4^+ can accumulate because of its incomplete oxidation. In stratified basins, segregation takes place between a nitrate reservoir in the oxygenated part of the water column and an ammonium reservoir in the anoxic part. In this case, loss of nitrogen occurs at the chemocline due to the combined effect of bacterial denitrification process and anaerobic oxidation of ammonia (anammox process), converting NO_3^- into gaseous species (N_2 and N_2O). If denitrification processes occurring at the redoxcline progress to completion, the subsequent deficit of N in the photic zone promotes the development of atmosphere-N_2 fixers (diazotrophs), including cyanobacteria (Sigman et al., 2005). A dominance of N fixation by diazotrophs drives $\delta^{15}N_{NO3}$- of surface waters toward 0‰ (Quan and Falkowski, 2009) resulting in sedimentary $\delta^{15}N$ values close to 0‰ during in the modern anoxic Black Sea or generally during the anoxic periods of the Phanerozoic (Ader et al., 2014; 2016; Algeo et al., 2014). In expanded oxygen minimum zones as observed in today's upwelling settings, or as proposed within the late Neoproterozoic ocean (Ader et al., 2014; 2016), a part of the NO_3^- is partially or quantitatively denitrified, inducing an increasing of the $\delta^{15}N$ composition of the residual NO_3^- pool toward a +12‰ value (Tesdal et al., 2013).

At Lambruisse, intervals characterized by anoxic conditions consistently record low $\delta^{15}N$ values (Fig. 3). Those intervals represent therefore periods of increased diazotrophy compensating a

587 decreasing in the N bioavailability that would have resulted from the establishment of a stratification
588 of the water-column during those periods. The frequent oscillations of $\delta^{15}N$ values observed in TH1
589 and TH3 imply that this stratification was relatively unstable. The relationship between $\delta^{15}N$ and TOC
590 (Fig. 7A) and HI (Fig. 7B) indicates that the burial of marine organic matter in the sediments (TOC >
591 1.0 wt% and HI > 200 mg HC/g TOC) was mainly enabled by its preservation under anoxic bottom
592 waters. This relationship between N_2 fixation in surface waters and bottom water deoxygenation is
593 confirmed by the negative correlation between $\delta^{15}N$ and EF V (Fig. 7D).

594 In addition, $\delta^{15}N$ was negatively correlated with the C_{org}/N_{bulk} molar ratio of the carbonate-free
595 samples (Fig. 7C). While the highest $\delta^{15}N$ values are consistent with "normal" marine OM (C/N = ~5-
596 8; Redfield ratio = 6.625), ^{15}N depletion is associated with increased C_{org}/N_{bulk} values towards typical
597 terrestrial OM (C/N > 25; Meyers, 1994). The dichotomy between high C_{org}/N_{bulk} values measured and
598 the presence of an interpreted dominant marine-derived OM with low $\delta^{15}N$, which characterize phases
599 of perturbation of the nitrogen cycle, has been explained by a complete denitrification occurring at the
600 redoxcline located within the water-column, combined with cyanobacterial nitrogen fixation in the
601 photic zone (e.g. Junium and Arthur, 2007). Experiments on denitrifying bacteria demonstrated the
602 preferential degradation of proteinaceous compounds, rich in N, as a source of carbon, leaving the OM
603 depleted in N and resulting in the high C/N preserved ratio (van Mooy et al., 2002). Besides, algal
604 biomass could presents a C/N ratio in excess of the Redfield-ratio as observed in modern settings with
605 N-limited surface-waters (e.g. Copin-Montégut, 2000). Another explanation for elevated C_{org}/N_{bulk} is
606 that a part of the ammonium accumulated in the clay fraction exceeded its retention capacity and
607 migrated out the sediments. Conversely, low C_{org}/N_{bulk} could be attributed to preferential preservation
608 of organic N as clay-adsorbed ammonium.

609 At Lambruisse, elevated C_{org}/N_{bulk} was observed in the dark shale intervals and the lowest
610 C_{org}/N_{bulk} within carbonates (Fig. 3). The impact of the clay fraction on the C_{org}/N_{bulk} ratio is therefore
611 minimal. Thus we consider that, at Lambruisse, the elevated C_{org}/N_{bulk} ratios, coherent with low $\delta^{15}N$
612 values, reflect the alteration of a Redfield-ratio organic matter pool, caused by intense denitrification
613 in the water-column and sediments.
614

615 **5.3. Integration of the Vocontian Basin in the regional nitrogen cycle**

616 During OAE 2, the development of cyanobacteria in the photic zone is deducted from the
617 preservation of methylhopanoids in the Central Atlantic (Kuypers et al., 2004; van Bentum et al.,
618 2012b), Lower Saxony Basin (Blumenberg and Wiese, 2012) and Levant Basin (Sepúlveda et al.,
619 2009). Thus, low $\delta^{15}N$ values associated with OAE 2 may be related to increasing cyanobacterial N_2
620 fixation at global scale (Kuypers et al., 2004; Ohkouchi et al., 2006; Junium and Arthur, 2007).

621 The similarity between the $\delta^{15}N$ vs. TOC trend at diverse OAE 2 sites and at Lambruisse
622 suggests that the scenario leading to diazotrophy in the photic zone is also consistent in the Vocontian

Basin (Fig. 8). However, this interpretation is challenged because bacterial N_2 fixation (involving the enzyme nitrogenase) is only accompanied by a 0 to -2‰ fractionation from a slightly positive isotope composition of dissolved N_2 (Zhang et al., 2014). Measured $\delta^{15}N$ values lower than -2‰, particularly those detected in the southern Central Atlantic (Fig. 8) (Kuypers et al., 2004; Junium and Arthur, 2007; Higgins et al., 2012; Ruvalcaba Baroni et al., 2015), have been explained by a change in the metal at the active site of the nitrogenase, from a classic Mo-nitrogenase to Fe- or V-nitrogenase, causing higher fractionation (Zerkle et al., 2008; Zhang et al., 2014). A change in biological nitrogen fixation could be related to a decrease of the global Mo concentration in seawater due to its uptake by sediments deposited in euxinic basins, as proposed for OAE 2 (Goldberg et al., 2016; Dickson et al., 2017). Another explanation for extreme negative $\delta^{15}N$ values involves a biological partial assimilation of NH_4^+ by phytoplankton in a sustained upwelling of bottom waters in the photic zone, which fuelled the primary productivity in N (Junium and Arthur, 2007; Higgins et al., 2012; Ruvalcaba Baroni et al., 2015). This NH_4^+ contribution proposed for southern Central Atlantic sites is compatible with the presence upwelling currents in this area (Trabucho Alexandre et al., 2010).

A high rate of phosphorus recycling during OAE 2 (Mort et al., 2007; Kraal et al., 2010), also suggested in the Vocontian Basin (Danzelle et al., 2018), has been interpreted as a consequence of OM decay and reductive dissolution of Fe-Mn-oxyhydroxides on which P is adsorbed (e.g. Ingall and Jahnke, 1994; Van Cappellen and Ingall, 1994; Dellwig et al., 2010). A positive feedback loop between primary productivity, increasing the oxygen demand in the water column, and P release in deoxygenated conditions and diffused back in the water column is interpreted as a requirement for maintaining anoxic conditions. In addition, phosphorus recycling combined with effective N loss due to intense denitrification process could have favoured N_2 fixation (Deutsch et al., 2004; Planavsky, 2014).

5.4. Paired carbon isotopes constraints on the carbon cycle

The relationship between the surficial global carbon cycle reflected in the OAE 2 sedimentary carbon isotope excursion and the long-term variations in TOC recorded at Lambruisse reveals a synchronicity between the global and the local expression of OAE 2. Variations in $\Delta^{13}C$ result from: (1) variations in the origin of OM with different initial $\delta^{13}C$ composition; or (2) variations in the kinetic fractionation associated with photosynthesis by primary producers, mostly controlled by the concentration of dissolved CO_2 in the ocean (Hayes et al., 1999).

At Lambruisse, chemical characterization of OM demonstrates an overwhelming dominance of marine-derived material (Fig. 5). This inference is in accordance with the palynology analysis of the Pont d'Issole section (Jarvis et al., 2011) indicating low terrestrial OM inputs, even during organic-poor intervals. Thus the $\Delta^{13}C$ record through the Lambruisse section could be interpreted as a pCO_2 indicator. The rising phase in $\Delta^{13}C$ at the base of the Niveau Thomel, recorded at Pont d'Issole (Jarvis et al., 2011), and represented at Lambruisse by the shift from lower $\Delta^{13}C$ values in the Pre-Thomel to

higher values in TH1 (Fig. 2), is interpreted as a consequence of the onset of CO_2 outgassing due to the emplacement of the Caribbean LIP at that time, also demonstrated by a drop in the Os isotope composition characterizing the hydrothermal activity of this LIP (Du Vivier et al., 2014).

The PCE interval is accompanied by low $\Delta^{13}C$ in the Lambruisse section (Fig. 2) as observed elsewhere in the Vocontian Basin (Pont d'Issole, Jarvis et al., 2011; Clot Chevalier, Gale et al., 2019), in the European Anglo-Paris and Saxony basins (Voigt et al., 2006; Jarvis et al., 2011) and in the Tarfaya basin (Moroccan Atlantic margin, Kuhnt et al., 2017). This event could be associated with a drop in marine and atmospheric CO_2 concentrations, explained by the massive quantities of organic carbon trapped in the sediments which act as a negative retroaction process for the carbon cycle (c.f. Jarvis et al., 2011).

The second rise after the PCE which culminate at around the CTB (Fig. 2), in parallel with the termination of the Os isotope excursion (Du Vivier et al., 2014), argues for continuous CO_2 outgassing during OAE 2. The termination of OAE 2 would mark a short drop in pCO_2 (Fig. 2) which could be one consequence of the second phase of carbon burial mostly corresponding with the TH3 unit.

Finally, the maximum $\Delta^{13}C$ values, observed during the Turonian (Fig. 2) indicate a continuous rise in the pCO_2 after the termination of OAE 2, implying that pCO_2 variations are not the only trigger of OAE 2. Thus, the burial of organic carbon, and subsequent cooling was not responsible for the termination of OAE 2, as proposed for the PCE. Robinson et al. (2019), proposed that a global sea-level rise combined with reduced nutrient delivery and hence reduced nutrient availability due to their sequestration in black shales would have favoured a decrease in productivity-supported or productivity-driven anoxic conditions.

5.5. Variations in paleotemperatures inferred from carbonate $\delta^{18}O$

Bulk carbonate $\delta^{18}O$ compositions were analyzed to assess changes in seawater temperature in the Vocontian Basin, and to compare them with the variations in pCO_2 identified from $\Delta^{13}C$ values. The absence of a positive correlation between $\delta^{13}C$ and $\delta^{18}O$ ($r^2 = 0.07$) throughout the Lambruisse section argues for the absence of a diagenetic alteration under meteoric conditions. Although $\delta^{18}O$ values can nevertheless shift to lower values during limited diagenesis, original trends may be preserved, making it possible to assess changes in seawater temperature, at least qualitatively (i.e. Jenkyns et al., 1994).

The absence of a clear $\delta^{18}O$ trend in the pre-OAE 2 interval suggests that sea-surface temperature remained relatively stable (Fig. 2). A positive $\delta^{18}O$ trend in TH2, with maximum values culminating at the TH2 – TH3 transition, around $\delta^{13}C$ peak "B", is interpreted here as a cooling phase associated with the PCE (Fig. 2). This interpretation implies the existence of a temporal lag in the record of maximum $\delta^{18}O$ values, in contrast to Boreal sections like Eastbourne (England; Paul et al., 1999), Gröbern (Germany; Voigt et al., 2006) or in the Western Interior Basin at Pueblo (Colorado;

Desmares et al., 2016) where the thermal minimum inferred from $\delta^{18}O$ is located around peak "A" (in PCE). Although quite erratic, the $\delta^{18}O$ signal roughly defines a long-term decrease after PCE, which we interpret as a general warming trend culminating at the top of the Niveau Thomel. This warming is coherent with the stratigraphic position of the early Turonian thermal maximum identified at Pont d'Issole and elsewhere in Europe (Jarvis et al., 2011), as well with the pCO_2 rise inferred from $\Delta^{13}C$ values (Fig. 2).

The absence of a large $\delta^{18}O$ positive excursion during the PCE in the Vocontian Basin is interpreted as less temperature sensitivity to variations in pCO_2 at subtropical latitudes than in the Boreal basins (Jarvis et al., 2011). We can also speculate that in the semi-enclosed Vocontian Basin, presumably characterized by a water-column stratification during OAE 2, variations in the evaporation vs. precipitation ratio may have affected the $\delta^{18}O$ composition of seawater, and consequently of carbonates.

Other sea temperature indicators in the Vocontian Basin confirm a cooling phase during the PCE. In the slope domain of the Vocontian Basin at Les Lattes, belemnites with a Boreal affinity have been reported within the stratigraphic interval of the PCE (Gale and Christensen, 1996). Grosheny et al. (2017) also described changes in the coiling-direction ratio of the planktonic foraminifera *Muricohedbergella delrioensis*, indicating that the transient cooling associated with the PCE was marked by the southward migration of Boreal species. What is more, sea-surface temperatures (SST) based on TEX_{86} values have been reported from the Cassis section in the South-Provençal Basin (Heimhofer et al., 2018), located immediately south of the Vocontian Basin (Fig. 1B). Most of the OAE2 interval is characterized by elevated SST of ~37 ± 2°C, interrupted by lower SST during the PCE reaching ~27°C at the end of this cooling episode. Based on the analysis of palynomorph abundances throughout this section, Heimhofer et al. (2018) described a mixed-forest vegetation, dominated by confiners indicating relatively humid conditions, during most of OAE2. Conversely, the PCE interval corresponds to a more open angiosperms-rich vegetation, likely representing the development of a savanna-type environment associated with a drier climate.

5.6. Global vs. local forcing mechanisms

In the Vocontian Basin, variations in the oxygen concentration in the sediments and in the water column over time were affected by both global and local forcing mechanisms at different timescale. During OAE 2, those variations are particularly evidenced at the scale of the lithological units. TH1 and TH3 periods (Fig. 9A) are distinctive to TH2 that broadly corresponds to PCE (Fig. 9B).

The tectonic confinement of the Vocontian Basin through the CTB (Grosheny et al., 2017) combined with the observation that black shales are restricted to the deepest part of the basin argues in favour of a semi-enclosed geometry of the Vocontian Basin. The EF Mo vs. EF U values measured at

Lambruisse are consistent with intermittent or weak particulate shuttle characterizing a fluctuating redoxcline within bottom waters (Tribovillard et al., 2012). During OAE 2, water-mass restriction is proposed as a major control for the establishment of anoxic conditions in different basins and particularly in the Central Atlantic where the most oxygen depletion was recorded (e.g. Monteiro et al., 2012).

The hypothesis that OAE 2 was triggered by a pulse of volcanic activity is widely supported in the literature (e.g. Turgeon and Creaser, 2008; Du Vivier et al., 2014; Adams et al., 2010; Jenkyns et al., 2017). A negative excursion of Os isotopes triggered ~50 kyr before OAE 2, which ended at the carbon isotope peak "B", was recorded at Pont d'Issole and worldwide (Du Vivier et al., 2014). An increase in pCO_2 is reflected in the increase in the $\Delta^{13}C$ record at the base of the Niveau Thomel (Jarvis et al., 2011) and has been linked to a global warming phase (Voigt et al., 2006; Forster et al., 2007; Sinninghe Damsté et al., 2010). The excess carbon in the ocean-atmosphere system was then regulated by the high rate of carbon burial in the form of OM, as recorded in the TH1 unit, and was further consumed as a reactant in the silicate weathering reaction (Blättler et al., 2011; Pogge von Strandmann et al., 2013). This would have led to the global transient cooling of the PCE, marked in Lambruisse by a drop in $\Delta^{13}C$ values followed by an increase in measured carbonate $\delta^{18}O$ values. Export of OM and associated oxygen consumption would have resulted in gradual oxygen depletion in bottom waters, marked by the enhanced preservation of OM and by enrichments in redox sensitive trace element (Mo, U, V, Zn). The inflow of boreal waters, associated with the PCE, could have promoted more efficient vertical mixing of the water column and intense reoxygenation of bottom waters in the Vocontian Basin.

Another consequence of volcanic activity is the degassing of large quantities of sulfate in the sulfate-poor Cenomanian oceans (Adams et al., 2010; Gomes et al., 2016). This would have promoted a higher rate of bacterial sulfate-reduction in sediments not limited by the availability of either sulfate or organic compounds (Poulton et al., 2015). Elevated rates of pyritization in the Vocontian Basin would have inhibited the burial of P sorbed onto Fe-oxyhydroxides, leading to significant P recycling in the water column (Danzelle et al., 2018). The resulting imbalanced N/P ratio would have been further strengthened by intermittent phases of enhanced water-column denitrification, in parallel with the oscillations in oxygenation of bottom waters, and favoured the development of nitrogen fixing cyanobacteria, thereby increasing primary productivity during OAE 2.

6. Conclusions

Our new data suggest that the development and evolution of OAE 2 in the Vocontian Basin could have resulted from a combination of exogenous mechanisms (volcanism, climate, tectonic) perturbing the hydrology of the Vocontian Basin and biogeochemical cycling. The moderately elevated concentrations of redox-sensitive trace elements and TOC reflect the establishment of

suboxic to anoxic conditions in the bottom waters in units TH1 and TH3. A relative higher enrichment in Mo than in U is consistent with the semi-enclosed geometry of the Vocontian Basin which favours the development of a stratified water body. The absence of noticeable enrichments in elements such as Ba, Ni and Cu suggests that surface waters in the Vocontian Basin did not experience eutrophic conditions, but rather episodic phases of moderately enhanced productivity.

Low sedimentary $\delta^{15}N$ values correlated with phases of bottom-water deoxygenation indicate periods of perturbation in the N cycle, characterized by the development of N_2-fixing cyanobacteria in the photic-zone. N_2-fixation indicates partial loss of bioavailable N caused by a high water-column denitrification rate, and a redoxcline located in the water column.

Phases of enhanced weathering conditions on land during periods of elevated pCO_2, supporting P transport and possible P recycling from deoxygenated bottom waters, would have led to low N/P availability for primary productivity, further favouring atmospheric N_2 fixation. Additional cyanobacterial production and the resulting increased export of marine OM would have acted as a positive feedback loop sustaining deoxygenation of the bottom waters.

The Plenus Cold Event, representing a cooler and drier climate phase, is characterized by a long-term reoxygenation of the Vocontian Basin. The massive burial of organic carbon during the early phase of OAE 2 may have led to lower pCO_2 at the global scale. This cooling phase may have modified ocean circulation and led to efficient mixing of the water column and ventilation of bottom waters.

Acknowledgments

Special thanks to Magali Ader and Hans-Jürgen Brumsack for useful discussions which helped us improve our papaer. We are grateful to Thomas J. Algeo, Ian Jarvis and the anonymous reviewer for providing insightful comments and constructive suggestions. We are also grateful to Théophile Cocquerez, Olivier Mathieu, and Anne-Lise Santoni at the University of Bourgogne-Franche-Comté for help with isotope geochemistry analyses and to Florence Savignac at Sorbonne University for Rock-Eval analyses. We thank Morgan Thomas and Armand Metghalchi, Master's student who help acquire the Rock-Eval data. This study was funded by the project Anox-Sea ANR-12-BS06-0011 coordinated by Emmanuelle Pucéat.

References

Adams, D.D., Hurtgen, M.T., Sageman, B.B., 2010. Volcanic triggering of a biogeochemical cascade during Oceanic Anoxic Event 2. Nat. Geosci. 3, 201–204. https://doi.org/10.1038/ngeo743

Ader, M., Sansjofre, P., Halverson, G.P., Busigny, V., Trindade, R.I.F., Kunzmann, M., Nogueira, A.C.R., 2014. Ocean redox structure across the Late Neoproterozoic Oxygenation Event: A nitrogen isotope perspective. Earth Planet. Sci. Lett. 396, 1–13. https://doi.org/10.1016/j.epsl.2014.03.042

Ader, M., Thomazo, C., Sansjofre, P., Busigny, V., Papineau, D., Laffont, R., Cartigny, P., Halverson, G.P., 2016. Interpretation of the nitrogen isotopic composition of Precambrian sedimentary rocks: Assumptions and perspectives. Chem. Geol. 429, 93–110. https://doi.org/10.1016/j.chemgeo.2016.02.010

Algeo, T., Meyers, P., Robinson, R., Rowe, H., Jiang, G., 2014. Icehouse–Greenhouse variations in marine denitrification. Biogeosciences, 11(4), 1273-1295. https://doi.org/10.5194/bg-11-1273-2014

Algeo, T.J., Maynard, J.B., 2004. Trace-element behavior and redox facies in core shales of Upper Pennsylvanian Kansas-type cyclothems. Chem. Geol., 206, 289–318. https://doi.org/10.1016/j.chemgeo.2003.12.009

Algeo, T.J., Rowe, H., 2012. Paleoceanographic applications of trace-metal concentration data. Chem. Geol. 324–325, 6–18. https://doi.org/10.1016/j.chemgeo.2011.09.002

Algeo, T.J., Tribovillard, N., 2009. Environmental analysis of paleoceanographic systems based on molybdenum–uranium covariation. Chem. Geol. 268, 211–225. https://doi.org/10.1016/j.chemgeo.2009.09.001

Arnaboldi, M., Meyers, P.A., 2007. Trace element indicators of increased primary production and decreased water-column ventilation during deposition of latest Pliocene sapropels at five locations across the Mediterranean Sea. Palaeogeogr. Palaeoclimatol. Palaeoecol. 249, 425–443. https://doi.org/10.1016/j.palaeo.2007.02.016

Arthur, M.A., Sageman, B.B., 1994. Marine Black Shales: Depositional Mechanisms and Environments of Ancient Deposits. Annu. Rev. Earth Planet. Sci. 22, 499–551. https://doi.org/10.1146/annurev.ea.22.050194.002435

Arthur, M.A., Dean, W.E., Pratt, L.M., 1988. Geochemical and climatic effects of increased marine organic carbon burial at the Cenomanian/Turonian boundary. Nature 335, 714–717. https://doi.org/10.1038/335714a0

Barclay, R.S., McElwain, J.C., Sageman, B.B., 2010. Carbon sequestration activated by a volcanic CO2 pulse during Ocean Anoxic Event 2. Nat. Geosci. 3, 205–208. https://doi.org/10.1038/ngeo757

Behar, F., Beaumont, V., de Penteado, H.L., 2001. Rock-Eval 6 technology: Performances and developments. Oil and Gas Science and Technology 56, 111-134.

Beil, S., Kuhnt, W., Holbourn, A., Scholz, F., Oxmann, J., Wallmann, K., Lorenzen, J., Aquit, M., Chellai, E.H., 2019. Cretaceous Oceanic Anoxic Events prolonged by phosphorus cycle feedbacks. Climate of the Past Discussions 1–42. https://doi.org/10.5194/cp-2019-118

Bice, K.L., Birgel, D., Meyers, P.A., Dahl, K.A., Hinrichs, K.-U., Norris, R.D., 2006. A multiple proxy and model study of Cretaceous upper ocean temperatures and atmospheric CO2 concentrations. Paleoceanography 21, PA2002. https://doi.org/10.1029/2005PA001203

Blakey, R. 2011. Global paleogeography. NAU Geology. http://deeptimemaps.com

Blättler, C.L., Jenkyns, H.C., Reynard, L.M., Henderson, G.M., 2011. Significant increases in global weathering during Oceanic Anoxic Events 1a and 2 indicated by calcium isotopes. Earth Planet. Sci. Lett. 309, 77–88. https://doi.org/10.1016/j.epsl.2011.06.029

Blumenberg, M., Wiese, F., 2012. Imbalanced nutrients as triggers for black shale formation in a shallow shelf setting during the OAE 2 (Wunstorf, Germany). Biogeosciences 9, 4139–4153. https://doi.org/10.5194/bg-9-4139-2012

Boyle, E.A., Sclater, F.R., Edmond, J.M., 1977. The distribution of dissolved copper in the Pacific. Earth Planet. Sci. Lett. 37, 38–54. https://doi.org/10.1016/0012-821X(77)90144-3

Brumsack, H.-J., 2006. The trace metal content of recent organic carbon-rich sediments: Implications for Cretaceous black shale formation. Palaeogeogr. Palaeoclimatol. Palaeoecol. 232, 344–361. https://doi.org/10.1016/j.palaeo.2005.05.011

Calvert, S.E., Pedersen, T.F., 1993. Geochemistry of Recent oxic and anoxic marine sediments: Implications for the geological record. Mar. Geol. 113, 67–88. https://doi.org/10.1016/0025-3227(93)90150-T

Carignan, J., Hild, P., Mevelle, G., Morel, J., Yeghicheyan, D., 2001. Routine Analyses of Trace Elements in Geological Samples using Flow Injection and Low Pressure On-Line Liquid Chromatography Coupled to ICP-MS: A Study of Geochemical Reference Materials BR,

DR-N, UB-N, AN-G and GH. Geostandards Newsletter 25, 187–198. https://doi.org/10.1111/j.1751-908X.2001.tb00595.x

Charbonnier, G., Adatte, T., Spangenberg, J.E., Föllmi, K.B., 2018. The expression of early Aptian to latest Cenomanian oceanic anoxic events in the sedimentary record of the Briançonnais domain. Glob. Planet. Change 170, 76–92. https://doi.org/10.1016/j.gloplacha.2018.08.009

Clarke, L.J., Jenkyns, H.C., 1999. New oxygen isotope evidence for long-term Cretaceous climatic change in the Southern Hemisphere. Geology 27, 699. https://doi.org/10.1130/0091-7613(1999)027<0699:NOIEFL>2.3.CO;2

Copin-Montégut, C., 2000. Consumption and production on scales of a few days of inorganic carbon, nitrate and oxygen by the planktonic community: results of continuous measurements at the Dyfamed Station in the northwestern Mediterranean Sea (May 1995). Deep Sea Research Part I: Oceanographic Research Papers 47, 447–477. https://doi.org/10.1016/S0967-0637(99)00098-9

Crumière, J.-P., 1989. Crise anoxique à la limite Cénomanien-Turonien dans le bassin subalpin oriental (Sud-Est de la France). Relation avec l'eustatisme. Geobios, Les Evenements de la Partie Moyenne du Cretache (Aptien a Turonien) 22, 189–203. https://doi.org/10.1016/S0016-6995(89)80056-7

Crumière, J.-P., Crumière-Airaud, C., Espitalié, J., Cotillon, P., 1990. Global and regional controls on potential source-rock deposition and preservation: The Cenomanian-Turonian Oceanic Anoxic Event (CTOAE) on the European Tethyan margin (southeastern France), in Deposition of Organic Facies, edited by A.Y. Huc, AAPG Stud. Geol. 30, 107-118.

Crusius, J., Calvert, S., Pedersen, T., Sage, D., 1996. Rhenium and molybdenum enrichments in sediments as indicators of oxic, suboxic and sulfidic conditions of deposition. Earth Planet. Sci. Lett. 145, 65–78. https://doi.org/10.1016/S0012-821X(96)00204-X

Danzelle, J., Riquier, L., Baudin, F., Thomazo, C., Pucéat, E., 2018. Oscillating redox conditions in the Vocontian Basin (SE France) during Oceanic Anoxic Event 2 (OAE 2). Chem. Geol. https://doi.org/10.1016/j.chemgeo.2018.05.039

Dellwig, O., Leipe, T., März, C., Glockzin, M., Pollehne, F., Schnetger, B., Yakushev, E.V., Böttcher, M.E., Brumsack, H.-J., 2010. A new particulate Mn–Fe–P-shuttle at the redoxcline of anoxic basins. Geochim. Cosmochim. Acta 74, 7100–7115. https://doi.org/10.1016/j.gca.2010.09.017

Desmares, D., Crognier, N., Bardin, J., Testé, M., Beaudoin, B., Grosheny, D., 2016. A new proxy for Cretaceous paleoceanographic and paleoclimatic reconstructions: Coiling direction changes in the planktonic foraminifera *Muricohedbergella delrioensi*s. Palaeogeogr. Palaeoclimatol. Palaeoecol. 445, 8–17. https://doi.org/10.1016/j.palaeo.2015.12.021

Deutsch, C., Sigman, D.M., Thunell, R.C., Meckler, A.N., Haug, G.H., 2004. Isotopic constraints on glacial/interglacial changes in the oceanic nitrogen budget. Glob. Biogeochem. Cycles 18. https://doi.org/10.1029/2003GB002189

Dickson, A.J., Jenkyns, H.C., Porcelli, D., van den Boorn, S., Idiz, E., 2016. Basin-scale controls on the molybdenum-isotope composition of seawater during Oceanic Anoxic Event 2 (Late Cretaceous). Geochim. Cosmochim. Acta 178, 291–306. https://doi.org/10.1016/j.gca.2015.12.036

Dickson, A.J., Saker-Clark, M., Jenkyns, H.C., Bottini, C., Erba, E., Russo, F., Gorbanenko, O., Naafs, B.D.A., Pancost, R.D., Robinson, S.A., van den Boorn, S.H.J., Idiz, E., 2017. A Southern Hemisphere record of global trace-metal drawdown and orbital modulation of organic-matter burial across the Cenomanian–Turonian boundary (Ocean Drilling Program Site 1138, Kerguelen Plateau). Sedimentology 64, 186–203. https://doi.org/10.1111/sed.12303

Donnadieu, Y., Pucéat, E., Moiroud, M., Guillocheau, F., Deconinck, J.-F., 2016. A better-ventilated ocean triggered by Late Cretaceous changes in continental configuration. Nat Commun 7, 10316. https://doi.org/10.1038/ncomms10316

Du Vivier, A.D.C., Selby, D., Sageman, B.B., Jarvis, I., Gröcke, D.R., Voigt, S., 2014. Marine $^{187}Os/^{188}Os$ isotope stratigraphy reveals the interaction of volcanism and ocean circulation during Oceanic Anoxic Event 2. Earth Planet. Sci. Lett. 389, 23–33. https://doi.org/10.1016/j.epsl.2013.12.024

Du Vivier, A.D.C., Selby, D., Condon, D.J., Takashima, R., Nishi, H., 2015. Pacific 187Os/188Os isotope chemistry and U–Pb geochronology: Synchroneity of global Os isotope change across OAE 2. Earth Planet. Sci. Lett. 428, 204–216. https://doi.org/10.1016/j.epsl.2015.07.020

Eldrett, J.S., Minisini, D., Bergman, S.C., 2014. Decoupling of the carbon cycle during Ocean Anoxic Event 2. Geology 42, 567–570. https://doi.org/10.1130/G35520.1

Eldrett, J.S., Ma, C., Bergman, S.C., Lutz, B., Gregory, F.J., Dodsworth, P., Phipps, M., Hardas, P., Minisini, D., Ozkan, A., Ramezani, J., Bowring, S.A., Kamo, S.L., Ferguson, K., Macaulay, C., Kelly, A.E., 2015. An astronomically calibrated stratigraphy of the Cenomanian, Turonian and earliest Coniacian from the Cretaceous Western Interior Seaway, USA: Implications for global chronostratigraphy. Cretac. Res. 56, 316–344. https://doi.org/10.1016/j.cretres.2015.04.010

Erbacher, J., Friedrich, O., Wilson, P.A., Birch, H., Mutterlose, J., 2005. Stable organic carbon isotope stratigraphy across Oceanic Anoxic Event 2 of Demerara Rise, western tropical Atlantic: Carbon isotope stratigraphy. Geochem. Geophys. Geosystems 6. https://doi.org/10.1029/2004GC000850

Espitalié, J., Deroo, G., Marquis, F., 1985a. La pyrolyse Rock-Eval et ses applications, Première partie. Revue de l'Institut Français du Pétrole 40, 563–579.

Espitalié, J., Deroo, G., Marquis, F., 1985b. La pyrolyse Rock-Eval et ses applications, Deuxième partie. Revue de l'Institut Français du Pétrole 40, 755–784.

Espitalié, J., Deroo, G., Marquis, F., 1986. La pyrolyse Rock-Eval et ses applications, Troisième partie. Revue de l'Institut Français du Pétrole, 41, 73–89.

Forster, A., Schouten, S., Moriya, K., Wilson, P.A., Sinninghe Damsté, J.S., 2007. Tropical warming and intermittent cooling during the Cenomanian/Turonian oceanic anoxic event 2: Sea surface temperature records from the equatorial Atlantic. Paleoceanography 22, PA1219. https://doi.org/10.1029/2006PA001349

Friedrich, O., Erbacher, J., Mutterlose, J., 2006. Paleoenvironmental changes across the Cenomanian/Turonian Boundary Event (Oceanic Anoxic Event 2) as indicated by benthic foraminifera from the Demerara Rise (ODP Leg 207). Rev. Micropaléontologie 49, 121–139. https://doi.org/10.1016/j.revmic.2006.04.003

Friedrich, O., Norris, R.D., Erbacher, J., 2012. Evolution of middle to Late Cretaceous oceans—A 55 m.y. record of Earth's temperature and carbon cycle. Geology 40, 107–110. https://doi.org/10.1130/G32701.1

Gale, A., Christensen, W.K., Occurrence of the belemnite *Actinocamax plenus* in the Cenomanian of SE France and its significance. Bull. Geol. Soc. Den. 43, 68-77.

Gale, A.S., Jenkyns, H.C., Tsikos, H., van Breugel, Y., Sinninghe Damsté, J.S., Bottini, C., Erba, E., Russo, F., Falzoni, F., Petrizzo, M.R., Dickson, A.J., Wray, D.S., 2019. High-resolution bio- and chemostratigraphy of an expanded record of Oceanic Anoxic Event 2 (Late Cenomanian–Early Turonian) at Clot Chevalier, near Barrême, SE France (Vocontian Basin). Newsl. Stratigr. 97–129. https://doi.org/10.1127/nos/2018/0445

Goldberg, T., Poulton, S.W., Wagner, T., Kolonic, S.F., Rehkämper, M., 2016. Molybdenum drawdown during Cretaceous Oceanic Anoxic Event 2. Earth Planet. Sci. Lett. 440, 81–91. https://doi.org/10.1016/j.epsl.2016.02.006

Gomes, M.L., Hurtgen, M.T., Sageman, B.B., 2016. Biogeochemical sulfur cycling during Cretaceous oceanic anoxic events: A comparison of OAE1a and OAE2. Paleoceanography 31, 2015PA002869. https://doi.org/10.1002/2015PA002869

Grosheny, D., Beaudoin, B., Morel, L., Desmares, D., 2006. High-resolution biotratigraphy and chemostratigraphy of the Cenomanian/Turonian boundary event in the Vocontian Basin, southeast France. Cretac. Res. 27, 629–640. https://doi.org/10.1016/j.cretres.2006.03.005

Grosheny, D., Ferry, S., Lécuyer, C., Thomas, A., Desmares, D., 2017. The Cenomanian–Turonian Boundary Event (CTBE) on the southern slope of the Subalpine Basin (SE France) and its bearing on a probable tectonic pulse on a larger scale. Cretac. Res. 72, 39–65. https://doi.org/10.1016/j.cretres.2016.11.009

970 Hayes, J.M., Strauss, H., Kaufman, A.J., 1999. The abundance of 13C in marine organic matter and
971 isotopic fractionation in the global biogeochemical cycle of carbon during the past 800 Ma.
972 Chem. Geol. 161, 103–125. https://doi.org/10.1016/S0009-2541(99)00083-2
973 Heimhofer, U., Wucherpfennig, N., Adatte, T., Schouten, S., Schneebeli-Hermann, E., Gardin, S.,
974 Keller, G., Kentsch, S., Kujau, A., 2018. Vegetation response to exceptional global warmth
975 during Oceanic Anoxic Event 2. Nat. Commun. 9, 3832. https://doi.org/10.1038/s41467-018-
976 06319-6
977 Hetzel, A., Böttcher, M.E., Wortmann, U.G., Brumsack, H.-J., 2009. Paleo-redox conditions during
978 OAE 2 reflected in Demerara Rise sediment geochemistry (ODP Leg 207). Palaeogeogr.
979 Palaeoclimatol. Palaeoecol. 273, 302–328. https://doi.org/10.1016/j.palaeo.2008.11.005
980 Hetzel, A., März, C., Vogt, C., Brumsack, H.-J., 2011. Geochemical environment of Cenomanian -
981 Turonian black shale deposition at Wunstorf (northern Germany). Cretac. Res. 32, 480–494.
982 https://doi.org/10.1016/j.cretres.2011.03.004
983 Higgins, M.B., Robinson, R.S., Husson, J.M., Carter, S.J., Pearson, A., 2012. Dominant eukaryotic
984 export production during ocean anoxic events reflects the importance of recycled NH4+.
985 Proc. Natl. Acad. Sci. U. S. A. 109, 2269–2274. https://doi.org/10.1073/pnas.1104313109
986 Holmden, C., Jacobson, A.D., Sageman, B.B., Hurtgen, M.T., 2016. Response of the Cr isotope proxy
987 to Cretaceous Ocean Anoxic Event 2 in a pelagic carbonate succession from the Western
988 Interior Seaway. Geochim. Cosmochim. Acta. https://doi.org/10.1016/j.gca.2016.04.039
989 Ingall, E., Jahnke, R., 1994. Evidence for enhanced phosphorus regeneration from marine sediments
990 overlain by oxygen depleted waters. Geochim. Cosmochim. Acta 58, 2571–2575.
991 https://doi.org/10.1016/0016-7037(94)90033-7
992 Jarvis, I., Gale, A.S., Jenkyns, H.C., Pearce, M.A., 2006. Secular variation in Late Cretaceous carbon
993 isotopes: a new δ13C carbonate reference curve for the Cenomanian–Campanian (99.6–70.6
994 Ma). Geol. Mag. 143, 561–608. https://doi.org/10.1017/S0016756806002421
995 Jarvis, I., Lignum, J.S., Gröcke, D.R., Jenkyns, H.C., Pearce, M.A., 2011. Black shale deposition,
996 atmospheric CO2 drawdown, and cooling during the Cenomanian-Turonian Oceanic Anoxic
997 Event. Paleoceanography 26, PA3201. https://doi.org/10.1029/2010PA002081
998 Jefferies, R.P.S., 1962. The palaeoecology of the Actinocamax plenus Subzone (lowest Turonian) in
999 the Anglo-Paris Basin. Palaeontology. 4, 609–647.
1000 Jenkyns, H.C., 2010. Geochemistry of oceanic anoxic events. Geochem. Geophys. Geosystems 11,
1001 Q03004. https://doi.org/10.1029/2009GC002788
1002 Jenkyns, H.C., Dickson, A.J., Ruhl, M., van den Boorn, S.H.J.M., 2017. Basalt-seawater interaction,
1003 the Plenus Cold Event, enhanced weathering and geochemical change: deconstructing
1004 Oceanic Anoxic Event 2 (Cenomanian–Turonian, Late Cretaceous). Sedimentology 64, 16–
1005 43. https://doi.org/10.1111/sed.12305
1006 Jenkyns, H.C., Gale, A.S., Corfield, R.M., 1994. Carbon- and oxygen-isotope stratigraphy of the
1007 English Chalk and Italian Scaglia and its palaeoclimatic significance. Geol. Mag. 131, 1.
1008 https://doi.org/10.1017/S0016756800010451
1009 Jenkyns, H.C., Matthews, A., Tsikos, H., Erel, Y., 2007. Nitrate reduction, sulfate reduction, and
1010 sedimentary iron isotope evolution during the Cenomanian-Turonian oceanic anoxic event.
1011 Paleoceanography 22, PA3208. https://doi.org/10.1029/2006PA001355
1012 Jones, C.E., Jenkyns, H.C., 2001. Seawater Strontium Isotopes, Oceanic Anoxic Events, and Seafloor
1013 Hydrothermal Activity in the Jurassic and Cretaceous. Am. J. Sci. 301, 112–149.
1014 https://doi.org/10.2475/ajs.301.2.112
1015 Junium, C.K., Arthur, M.A., 2007. Nitrogen cycling during the Cretaceous, Cenomanian-Turonian
1016 Oceanic Anoxic Event II. Geochem. Geophys. Geosystems 8, Q03002.
1017 https://doi.org/10.1029/2006GC001328
1018 Kennedy, W.J., Walaszczyk, I., Cobban, W.A., 2005. The global boundary stratotype section and
1019 point for the base of the Turonian stage of the cretaceous: Pueblo, Colorado, U.S.A.
1020 Episodes 28. 93–104. https://doi.org/10.18814/epiiugs/2005/v28i2/003
1021 Kingsbury, C.G., Kamo, S.L., Ernst, R.E., Söderlund, U., Cousens, B.L., 2017. U-Pb geochronology
1022 of the plumbing system associated with the Late Cretaceous Strand Fiord Formation, Axel
1023 Heiberg Island, Canada: part of the 130-90 Ma High Arctic large igneous province. J.
1024 Geodyn. https://doi.org/10.1016/j.jog.2017.11.001

Kraal, P., Slomp, C.P., Forster, A., Kuypers, M.M.M., 2010. Phosphorus cycling from the margin to abyssal depths in the proto-Atlantic during oceanic anoxic event 2. Palaeogeogr. Palaeoclimatol. Palaeoecol. 295, 42–54. https://doi.org/10.1016/j.palaeo.2010.05.014

Kuhnt,W., Thurow, J., Wiedmann, J., Herbin, J.P.,1986. Oceanic anoxic conditions around the Cenomanian/Turonian boundary and the response of the biota. In: Degens, E.T., Meyers, P.A., Brassell, S.C. (Eds.), Biogeochemistry of Black Shales: Mitt.Geol.- Paläontol. Inst. Univ. Hamburg SCOPE/UNEP Sonderband Heft, vol. 60, pp. 205–246.

Kuhnt, W., Luderer, F., Nederbragt, S., Thurow, J., Wagner, T., 2004. Orbital-scale record of the late Cenomanian–Turonian oceanic anoxic event (OAE-2) in the Tarfaya Basin (Morocco). Int. J. Earth Sci. 94, 147–159. https://doi.org/10.1007/s00531-004-0440-5

Kuhnt, W., Holbourn, A.E., Beil, S., Aquit, M., Krawczyk, T., Flögel, S., Chellai, E.H., Jabour, H., 2017. Unraveling the onset of Cretaceous Oceanic Anoxic Event 2 in an extended sediment archive from the Tarfaya-Laayoune Basin, Morocco. Paleoceanography 32, 923–946. https://doi.org/10.1002/2017PA003146

Kuypers, M.M.M., Pancost, R.D., Nijenhuis, I.A., Sinninghe Damsté, J.S., 2002. Enhanced productivity led to increased organic carbon burial in the euxinic North Atlantic basin during the late Cenomanian oceanic anoxic event. Paleoceanography 17, 1051. https://doi.org/10.1029/2000PA000569

Kuypers, M.M.M., Breugel, Y. van, Schouten, S., Erba, E., Damsté, J.S.S., 2004. N2-fixing cyanobacteria supplied nutrient N for Cretaceous oceanic anoxic events. Geology 32, 853–856. https://doi.org/10.1130/G20458.1

MacLeod, K.G., Martin, E.E., Blair, S.W., 2008. Nd isotopic excursion across Cretaceous ocean anoxic event 2 (Cenomanian-Turonian) in the tropical North Atlantic. Geology 36, 811–814. https://doi.org/10.1130/G24999A.1

McLennan, S.M., 2001. Relationships between the trace element composition of sedimentary rocks and upper continental crust. Geochem. Geophys. Geosyst. 2, 1021. https://doi.org/10.1029/2000GC000109

McManus, J., Berelson, W.M., Klinkhammer, G.P., Johnson, K.S., Coale, K.H., Anderson, R.F., Kumar, N., Burdige, D.J., Hammond, D.E., Brumsack, H.J., McCorkle, D.C., Rushdi, A., 1998. Geochemistry of barium in marine sediments: implications for its use as a paleoproxy. Geochim. Cosmochim. Acta 62, 3453–3473. https://doi.org/10.1016/S0016-7037(98)00248-8

Meyers, P.A., 1994. Preservation of elemental and isotopic source identification of sedimentary organic matter. Chem. Geol. 114, 289–302. https://doi.org/10.1016/0009-2541(94)90059-0

Meyers, S.R., Sageman, B.B., Arthur, M.A., 2012. Obliquity forcing and the amplification of high-latitude climate processes during Oceanic Anoxic Event 2. Paleoceanography 27. https://doi.org/10.1029/2012PA002286

Monteiro, F.M., Pancost, R.D., Ridgwell, A., Donnadieu, Y., 2012. Nutrients as the dominant control on the spread of anoxia and euxinia across the Cenomanian-Turonian oceanic anoxic event (OAE2): Model-data comparison. Paleoceanography 27, PA4209. https://doi.org/10.1029/2012PA002351

Morel, L., 1998. Stratigraphie à haute résolution du passage Cénomanien-Turonien. Thèse de l'Université Pierre et Marie Curie, Paris VI, 224 pp.

Morford, J.L., Russell, A.D., Emerson, S., 2001. Trace metal evidence for changes in the redox environment associated with the transition from terrigenous clay to diatomaceous sediment, Saanich Inlet, BC. Mar. Geol. 174, 355–369. https://doi.org/10.1016/S0025-3227(00)00160-2

Morse, J.W., Luther, G.W., 1999. Chemical influences on trace metal-sulfide interactions in anoxic sediments. Geochim. Cosmochim. Acta 63, 3373–3378. https://doi.org/10.1016/S0016-7037(99)00258-6

Mort, H.P., Adatte, T., Föllmi, K.B., Keller, G., Steinmann, P., Matera, V., Berner, Z., Stüben, D., 2007. Phosphorus and the roles of productivity and nutrient recycling during oceanic anoxic event 2. Geology 35, 483–486. https://doi.org/10.1130/G23475A.1

O'Brien, C.L., Robinson, S.A., Pancost, R.D., Sinninghe Damsté, J.S., Schouten, S., Lunt, D.J., Alsenz, H., Bornemann, A., Bottini, C., Brassell, S.C., Farnsworth, A., Forster, A., Huber,

B.T., Inglis, G.N., Jenkyns, H.C., Linnert, C., Littler, K., Markwick, P., McAnena, A., Mutterlose, J., Naafs, B.D.A., Püttmann, W., Sluijs, A., van Helmond, N.A.G.M., Vellekoop, J., Wagner, T., Wrobel, N.E., 2017. Cretaceous sea-surface temperature evolution: Constraints from TEX86 and planktonic foraminiferal oxygen isotopes. Earth-Sci. Rev. 172, 224–247. https://doi.org/10.1016/j.earscirev.2017.07.012

Ohkouchi, N., Kashiyama, Y., Kuroda, J., Ogawa, N.O., Kitazato, H., 2006. The importance of diazotrophic cyanobacteria as primary producers during Cretaceous Oceanic Anoxic Event 2. Biogeosciences 3, 467–478. https://doi.org/10.5194/bg-3-467-2006

Owens, J.D., Lyons, T.W., Li, X., Macleod, K.G., Gordon, G., Kuypers, M.M.M., Anbar, A., Kuhnt, W., Severmann, S., 2012. Iron isotope and trace metal records of iron cycling in the proto-North Atlantic during the Cenomanian-Turonian oceanic anoxic event (OAE-2). Paleoceanography 27, PA3223. https://doi.org/10.1029/2012PA002328

Parente, M., Frijia, G., Di Lucia, M., Jenkyns, H.C., Woodfine, R.G., Baroncini, F., 2008. Stepwise extinction of larger foraminifers at the Cenomanian-Turonian boundary: A shallow-water perspective on nutrient fluctuations during Oceanic Anoxic Event 2 (Bonarelli Event). Geology 36, 715. https://doi.org/10.1130/G24893A.1

Paul, C.R.C., Lamolda, M.A., Mitchell, S.F., Vaziri, M.R., Gorostidi, A., Marshall, J.D., 1999. The Cenomanian–Turonian boundary at Eastbourne (Sussex, UK): a proposed European reference section. Palaeogeogr. Palaeoclimatol. Palaeoecol. 150, 83–121. https://doi.org/10.1016/S0031-0182(99)00009-7

Pearce, M.A., Jarvis, I., Tocher, B.A., 2009. The Cenomanian–Turonian boundary event, OAE2 and palaeoenvironmental change in epicontinental seas: New insights from the dinocyst and geochemical records. Palaeogeogr. Palaeoclimatol. Palaeoecol. 280, 207–234. https://doi.org/10.1016/j.palaeo.2009.06.012

Percival, L., 2018. Does large igneous province volcanism always perturb the mercury cycle? Comparing the records of Oceanic Anoxic Event 2 and the end-Cretaceous to other Mesozoic events.

Peters, K., 1986. Guidelines for Evaluating Petroleum Source Rock Using Programmed Pyrolysis. https://doi.org/10.1306/94885688-1704-11D7-8645000102C1865D

Philip, J., Babinot, J. F., Tronchetti, G., Fourcade, E., Guiraud, R., Bellion, Y., Herbin, J. P., Combes, P. J., Cornee, J. J., Dercourt, J., and Ricou, L. E., 1993. Late Cenomanian (94-92 Ma), in: Atlas Tethys Palaeoenvironmental Maps. Explanatory Notes, 153–178, (J. Dercourt, L. E. Ricou, and B. Vrielynck, eds.) Gauthier-Villars, Paris.

Planavsky, N.J., 2014. The elements of marine life. Nat. Geosci. 7, 855. https://doi.org10.1038/ngeo2307

Pogge von Strandmann, P.A.E., Jenkyns, H.C., Woodfine, R.G., 2013. Lithium isotope evidence for enhanced weathering during Oceanic Anoxic Event 2. Nat. Geosci. 6, 668–672. https://doi.org/10.1038/ngeo1875

Porthault, B., 1974. Le Crétacé supérieur de la Fosse vocontienne et des régions limitrophes : (France sud-est), micropaléontologie, stratigraphie, paléogéographie (phdthesis). Université Claude Bernard - Lyon I.

Poulton, S.W., Henkel, S., März, C., Urquhart, H., Flögel, S., Kasten, S., Damsté, J.S.S., Wagner, T., 2015. A continental-weathering control on orbitally driven redox-nutrient cycling during Cretaceous Oceanic Anoxic Event 2. Geology 43, 963–966. https://doi.org/10.1130/G36837.1

Pucéat, E., Lécuyer, C., Sheppard, S.M.F., Dromart, G., Reboulet, S., Grandjean, P., 2003. Thermal evolution of Cretaceous Tethyan marine waters inferred from oxygen isotope composition of fish tooth enamels. Paleoceanography 18, 1029. https://doi.org/10.1029/2002PA000823

Raven, M.R., Fike, D.A., Gomes, M.L., Webb, S.M., Bradley, A.S., McClelland, H.-L.O., 2018. Organic carbon burial during OAE 2 driven by changes in the locus of organic matter sulfurization. Nat. Commun. 9, 3409. https://doi.org/10.1038/s41467-0181-05943-6

Raven, M.R., Fike, D.A., Bradley, A.S., Gomes, M.L., Owens, J.D., Webb, S.A., 2019. Paired organic matter and pyrite δ34S records reveal mechanisms of carbon, sulfur, and iron cycle disruption during Ocean Anoxic Event 2. Earth Planet. Sci. Lett. 512, 27–38. https://doi.org/10.1016/j.epsl.2019.01.048

Riquier, L., Tribovillard, N., Averbuch, O., Devleeschouwer, X., Riboulleau, A., 2006. The Late Frasnian Kellwasser horizons of the Harz Mountains (Germany): Two oxygen-deficient periods resulting from different mechanisms. Chem. Geol. 233, 137–155. https://doi.org/10.1016/j.chemgeo.2006.02.021

Robinson, S.A., Dickson, A.J., Pain, A., Jenkyns, H.C., O'Brien, C.L., Farnsworth, A., Lunt, D.J., 2019. Southern Hemisphere sea-surface temperatures during the Cenomanian–Turonian: Implications for the termination of Oceanic Anoxic Event 2. Geology 47, 131–134. https://doi.org/10.1130/G45842.1

Ruvalcaba Baroni, I., van Helmond, N. a. G.M., Tsandev, I., Middelburg, J.J., Slomp, C.P., 2015. The nitrogen isotope composition of sediments from the proto-North Atlantic during Oceanic Anoxic Event 2. Paleoceanography 30, 2014PA002744. https://doi.org/10.1002/2014PA002744

Sageman, B.B., Meyers, S.R., Arthur, M.A., 2006. Orbital time scale and new C-isotope record for Cenomanian-Turonian boundary stratotype. Geology 34, 125–128. https://doi.org/10.1130/G22074.1

Scaife, J.D., Ruhl, M., Dickson, A.J., Mather, T.A., Jenkyns, H.C., Percival, L.M.E., Hesselbo, S.P., Cartwright, J., Eldrett, J.S., Bergman, S.C., Minisini, D., 2017. Sedimentary Mercury Enrichments as a Marker for Submarine Large Igneous Province Volcanism? Evidence From the Mid-Cenomanian Event and Oceanic Anoxic Event 2 (Late Cretaceous). Geochemistry, Geophysics, Geosystems 18, 4253–4275. https://doi.org/10.1002/2017gc007153

Schlanger, S.O., Jenkyns, H.C., 1976. Cretaceous anoxic events: causes and consequences. Geol. Mijnb. 55, 179–184.

Scopelliti, G., Bellanca, A., Erba, E., Jenkyns, H.C., Neri, R., Tamagnini, P., Luciani, V., Masetti, D., 2008. Cenomanian–Turonian carbonate and organic-carbon isotope records, biostratigraphy and provenance of a key section in NE Sicily, Italy: Palaeoceanographic and palaeogeographic implications. Palaeogeogr. Palaeoclimatol. Palaeoecol. 265, 59–77. https://doi.org/10.1016/j.palaeo.2008.04.022

Sepúlveda, J., Wendler, J., Leider, A., Kuss, H.-J., Summons, R.E., Hinrichs, K.-U., 2009. Molecular isotopic evidence of environmental and ecological changes across the Cenomanian–Turonian boundary in the Levant Platform of central Jordan. Org. Geochem. 40, 553–568. https://doi.org/10.1016/j.orggeochem.2009.02.009

Sigman, D.M., Granger, J., DiFiore, P.J., Lehmann, M.M., Ho, R., Cane, G., van Geen, A., 2005. Coupled nitrogen and oxygen isotope measurements of nitrate along the eastern North Pacific margin: N and O isotopes of nitrate along the North Pacific margin. Glob. Biogeochem. Cycles 19, GGB4022. https://doi.org/10.1029/2005GB002458

Sinninghe Damsté, J.S.S., Kuypers, M.M.M., Pancost, R.D., Schouten, S., 2008. The carbon isotopic response of algae, (cyano)bacteria, archaea and higher plants to the late Cenomanian perturbation of the global carbon cycle: Insights from biomarkers in black shales from the Cape Verde Basin (DSDP Site 367). Org. Geochem., Stable Isotopes in Biogeosciences (II) 39, 1703–1718. https://doi.org/10.1016/j.orggeochem.2008.01.012

Sinninghe Damsté, J.S., van Bentum, E.C., Reichart, G.-J., Pross, J., Schouten, S., 2010. A CO2 decrease-driven cooling and increased latitudinal temperature gradient during the mid-Cretaceous Oceanic Anoxic Event 2. Earth Planet. Sci. Lett. 293, 97–103. https://doi.org/10.1016/j.epsl.2010.02.027

Sinton, C.W., Duncan, R.A., 1997. Potential links between ocean plateau volcanism and global ocean anoxia at the Cenomanian-Turonian boundary. Econ. Geol. 92, 836–842. https://doi.org/10.2113/gsecongeo.92.7-8.836

Snow, L.J., Duncan, R.A., Bralower, T.J., 2005. Trace element abundances in the Rock Canyon Anticline, Pueblo, Colorado, marine sedimentary section and their relationship to Caribbean plateau construction and oxygen anoxic event 2. Paleoceanography 20, PA3005. https://doi.org/10.1029/2004PA001093

Sweere, T.C., Dickson, A.J., Jenkyns, H.C., Porcelli, D., Elrick, M., Boorn, S.H.J.M. van den, Henderson, G.M., 2018. Isotopic evidence for changes in the zinc cycle during Oceanic Anoxic Event 2 (Late Cretaceous). Geology 46, 463–466. https://doi.org/10.1130/G40226.1

Takashima, R., Nishi, H., Hayashi, K., Okada, H., Kawahata, H., Yamanaka, T., Fernando, A.G., Mampuku, M., 2009. Litho-, bio- and chemostratigraphy across the Cenomanian/Turonian boundary (OAE 2) in the Vocontian Basin of southeastern France. Palaeogeogr. Palaeoclimatol. Palaeoecol. 273, 61–74. https://doi.org/10.1016/j.palaeo.2008.12.001

Taylor, S., McLennan, S., 1995. The Geochemical Evolution of the Continental-Crust. Rev. Geophys. 33, 241–265. https://doi.org/10.1029/95RG00262

Tegner, C., Storey, M., Holm, P.M., Thorarinsson, S.B., Zhao, X., Lo, C.-H., Knudsen, M.F., 2011. Magmatism and Eurekan deformation in the High Arctic Large Igneous Province: 40Ar-39Ar age of Kap Washington Group volcanics, North Greenland. Earth Planet. Sci. Lett. 303, 203–214. https://doi.org/10.1016/j.epsl.2010.12.047

Tesdal, J.-E., Galbraith, E.D., Kienast, M., 2013. Nitrogen isotopes in bulk marine sediment: linking seafloor observations with subseafloor records. Biogeosciences 10, 101–118. https://doi.org/10.5194/bg-10-101-2013

Thomazo, C., Ader, M., Philippot, P., 2011. Extreme 15N-enrichments in 2.72-Gyr-old sediments: evidence for a turning point in the nitrogen cycle. Geobiology 9, 107–120. https://doi.org/10.1111/j.1472-4669.2011.00271.x

Trabucho Alexandre, J., Tuenter, E., Henstra, G.A., van der Zwan, K.J., van de Wal, R.S.W., Dijkstra, H.A., de Boer, P.L., 2010. The mid-Cretaceous North Atlantic nutrient trap: Black shales and OAEs. Paleoceanography 25, PA4201. https://doi.org/10.1029/2010PA001925

Tribovillard, N., Algeo, T.J., Baudin, F., Riboulleau, A., 2012. Analysis of marine environmental conditions based onmolybdenum–uranium covariation—Applications to Mesozoic paleoceanography. Chem. Geol. 324–325, 46–58. https://doi.org/10.1016/j.chemgeo.2011.09.009

Tribovillard, N., Algeo, T.J., Lyons, T., Riboulleau, A., 2006. Trace metals as paleoredox and paleoproductivity proxies: An update. Chem. Geol. 232, 12–32. https://doi.org/10.1016/j.chemgeo.2006.02.012

Tribovillard, N., Riboulleau, A., Lyons, T., Baudin, F., 2004a. Enhanced trapping of molybdenum by sulfurized marine organic matter of marine origin in Mesozoic limestones and shales. Chem. Geol. 213, 385–401. https://doi.org/10.1016/j.chemgeo.2004.08.011

Tribovillard, N., Trentesaux, A., Ramdani, A., Baudinet, F., Riboulleau, A., 2004b. Controls on organic accumulation in late Jurassic shales of northwestern Europe as inferred from trace-metal geochemistry. Bull. Société Géologique Fr. 491–506.

Tsandev, I., Slomp, C.P., 2009. Modeling phosphorus cycling and carbon burial during Cretaceous Oceanic Anoxic Events. Earth Planet. Sci. Lett. 286, 71–79. https://doi.org/10.1016/j.epsl.2009.06.016

Tsikos, H., Jenkyns, H.C., Walsworth-Bell, B., Petrizzo, M.R., Forster, A., Kolonic, S., Erba, E., Silva, I.P., Baas, M., Wagner, T., Damsté, J.S.S., 2004. Carbon-isotope stratigraphy recorded by the Cenomanian–Turonian Oceanic Anoxic Event: correlation and implications based on three key localities. J. Geol. Soc. 161, 711–719. https://doi.org/10.1144/0016-764903-077

Turgeon, S., Brumsack, H.-J., 2006. Anoxic vs dysoxic events reflected in sediment geochemistry during the Cenomanian–Turonian Boundary Event (Cretaceous) in the Umbria–Marche Basin of central Italy. Chem. Geol. 234, 321–339. https://doi.org/10.1016/j.chemgeo.2006.05.008

Turgeon, S.C., Creaser, R.A., 2008. Cretaceous oceanic anoxic event 2 triggered by a massive magmatic episode. Nature 454, 323–326. https://doi.org/10.1038/nature07076

van Bentum, E.C., Reichart, G.-J., Forster, A., Sinninghe Damsté, J.S., 2012a. Latitudinal differences in the amplitude of the OAE-2 carbon isotopic excursion: pCO2 and paleo productivity. Biogeosciences 9, 717–731. https://doi.org/10.5194/bg-9-717-2012

van Bentum, E.C., Reichart, G.-J., Sinninghe Damsté, J.S., 2012b. Organic matter provenance, palaeoproductivity and bottom water anoxia during the Cenomanian/Turonian oceanic anoxic event in the Newfoundland Basin (northern proto North Atlantic Ocean). Org. Geochem. 50, 11–18. https://doi.org/10.1016/j.orggeochem.2012.05.013

Van Cappellen, P., Ingall, E.D., 1994. Benthic phosphorus regeneration, net primary production, and ocean anoxia: A model of the coupled marine biogeochemical cycles of carbon and phosphorus. Paleoceanography 9, 677–692. https://doi.org/10.1029/94PA01455

Van Cappellen, P., Viollier, E., Roychoudhury, A., Clark, L., Ingall, E., Lowe, K., Dichristina, T., 1998. Biogeochemical Cycles of Manganese and Iron at the Oxic−Anoxic Transition of a Stratified Marine Basin (Orca Basin, Gulf of Mexico). Environ. Sci. Technol. 32, 2931–2939. https://doi.org/10.1021/es980307m

van Helmond, N.A.G.M., Ruvalcaba Baroni, I., Sluijs, A., Sinninghe Damsté, J.S., Slomp, C.P., 2014a. Spatial extent and degree of oxygen depletion in the deep proto-North Atlantic basin during Oceanic Anoxic Event 2. Geochem. Geophys. Geosystems 15, 4254–4266. https://doi.org/10.1002/2014GC005528

van Helmond, N.A.G.M., Sluijs, A., Reichart, G.-J., Damsté, J.S.S., Slomp, C.P., Brinkhuis, H., 2014b. A perturbed hydrological cycle during Oceanic Anoxic Event 2. Geology 42, 123–126. https://doi.org/10.1130/G34929.1

van Helmond, N.A.G.M., Sluijs, A., Sinninghe Damsté, J.S., Reichart, G.-J., Voigt, S., Erbacher, J., Pross, J., Brinkhuis, H., 2015. Freshwater discharge controlled deposition of Cenomanian–Turonian black shales on the NW European epicontinental shelf (Wunstorf, northern Germany). Clim Past 11, 495–508. https://doi.org/10.5194/cp-11-495-2015

van Helmond, N.A.G.M., Sluijs, A., Papadomanolaki, N.M., Plint, A.G., Gröcke, D.R., Pearce, M.A., Eldrett, J.S., Trabucho-Alexandre, J., Walaszczyk, I., van de Schootbrugge, B., Brinkhuis, H., 2016. Equatorward phytoplankton migration during a cold spell within the Late Cretaceous super-greenhouse. Biogeosciences 13, 2859–2872. https://doi.org/10.5194/bg-13-2859-2016

Voigt, S., Erbacher, J., Mutterlose, J., Weiss, W., Westerhold, T., Wiese, F., Wilmsen, M., Wonik, T., 2008. The Cenomanian – Turonian of the Wunstorf section – (North Germany): global stratigraphic reference section and new orbital time scale for Oceanic Anoxic Event 2. Newsl. Stratigr. 43, 65–89. https://doi.org/10.1127/0078-0421/2008/0043-0065

Voigt, S., Gale, A.S., Voigt, T., 2006. Sea-level change, carbon cycling and palaeoclimate during the Late Cenomanian of northwest Europe; an integrated palaeoenvironmental analysis. Cretac. Res. 27, 836–858. https://doi.org/10.1016/j.cretres.2006.04.005

Westermann, S., Vance, D., Cameron, V., Archer, C., Robinson, S.A., 2014. Heterogeneous oxygenation states in the Atlantic and Tethys oceans during Oceanic Anoxic Event 2. Earth Planet. Sci. Lett. 404, 178–189. https://doi.org/10.1016/j.epsl.2014.07.018

Zerkle, A.L., Junium, C.K., Canfield, D.E., House, C.H., 2008. Production of 15N-depleted biomass during cyanobacterial N2-fixation at high Fe concentrations. J. Geophys. Res. Biogeosciences 113. https://doi.org/10.1029/2007JG000651

Zhang, X., Gao, Y., Chen, X., Hu, D., Li, M., Wang, C., Shen, Y., 2019. Nitrogen isotopic composition of sediments from the eastern Tethys during Oceanic Anoxic Event 2. Palaeogeogr. Palaeoclimatol. Palaeoecol., Palaeogeographic, palaeoclimatic and palaeoecologic evolution of eastern Tethys during the Mesozoic and Cenozoic 515, 123-133. https://doi.org/10.1016/j.palaeo.2018.03.013

Zhang, X., Sigman, D.M., Morel, F.M.M., Kraepiel, A.M.L., 2014. Nitrogen isotope fractionation by alternative nitrogenases and past ocean anoxia. Proc. Natl. Acad. Sci. 111, 4782–4787. https://doi.org/10.1073/pnas.1402976111

Zheng, X.-Y., Jenkyns, H.C., Gale, A.S., Ward, D.J., Henderson, G.M., 2013. Changing ocean circulation and hydrothermal inputs during Ocean Anoxic Event 2 (Cenomanian–Turonian): Evidence from Nd-isotopes in the European shelf sea. Earth Planet. Sci. Lett. 375, 338–348. https://doi.org/10.1016/j.epsl.2013.05.053

Zheng, X.-Y., Jenkyns, H.C., Gale, A.S., Ward, D.J., Henderson, G.M., 2016. A climatic control on reorganization of ocean circulation during the mid-Cenomanian event and Cenomanian-Turonian oceanic anoxic event (OAE 2): Nd isotope evidence. Geology 44, 151–154. https://doi.org/10.1130/G37354.1

Figures and table captions

Figure 1

(A) Paleogeographic map at the Cenomanian of the Vocontian Basin and the South-Provençal Basin presenting the extension of the facies deposits (after Crumière et al., 1990). (B) Location of the Vocontian Basin sections referred to in the text (after Crumière et al., 1990).

Figure 2

Stratigraphic succession, TOC content and carbon- and oxygen-isotope compositions through the Lambruisse section. Descriptions of the lithological units (TH1 to TH4) forming the Niveau Thomel are provided in the text. OAE 2 interval is represented by the light grey band determined on the base of the positive carbon isotope excursion (characterized by three maxima A, B, C). Blue band represents the Plenus Cold Event (PCE) placed by stratigraphic correlation with European sections (Jarvis et al., 2011). Horizontal dark grey bands highlight the intervals of dark shale characterized by TOC values higher than or equal to 1.0 wt%.

Figure 3

Evolution of the N concentration, C_{org}/N_{bulk} molar ratio and nitrogen isotope composition of the decarbonated fraction through the Lambruisse section.

Figure 4

Evolution of the enrichment factors [EF X = $(X/Al)_{sample}/(X/Al)_{UCC}$] of the redox-sensitive trace elements (RSTE) with minimal detrital influence (Mo, V, U) and those associated with primary productivity (Zn, Ni, Cu, Ba) through the Lambruisse section.

Figure 5

Modified Van Krevelen diagram presenting Hydrogen Index (HI) versus Oxygen Index (OI) and the associated type of OM at Lambruisse. Only samples having TOC > 0.4 wt% are plotted.

Figure 6

EF Mo versus EF U for the Lambruisse (this study), Pont d'Issole (Danzelle et al., 2018) and Clot Chevalier (Gale et al., 2019) sections. Diagonal dashed lines represent the 3/1; 1/1 and 0.3/1 (Mo/U) ratios of present-day seawater. Area of yellow to red color gradient corresponds to the evolution of EF Mo vs. EF U under suboxic to euxinic conditions in modern unrestricted marine environments, based on eastern tropical Pacific locations (Tribovillard et al., 2012). Grey area corresponds to the values typical of "Particulate Shuttle" effect characteristic of weakly restricted basins (Tribovillard et al., 2012).

Figure 7

Nitrogen isotopes compositions versus (A) TOC, (B) HI, (C) C_{org}/N_{bulk} molar ratio and (D) EF V at Lambruisse. Greenish arrows represent the broad inverse trends observed.

Figure 8

(A) Palaeogeographic reconstruction at 90 Ma after Blakey (2011) with the location of the Lambruisse section in the Vocontian Basin and other sites discussed in the compilation of nitrogen isotope signals during OAE 2. (B) Nitrogen isotope compositions versus TOC for Lambruisse and compiled OAE 2 sites from the Lower Saxony Basin (Wunstorf section, Blumemberg and Wiese, 2012; Ruvalcaba Baroni et al., 2015), Central Atlantic (DSDP Site 367, Kuypers et al., 2004; Bass River section, DSDP Sites 386, 641, ODP Site 1276, Ruvalcaba Baroni et al., 2015), Western Tethys (Gorgo a Cerbara section, Ohkouchi et al., 2006) and Eastern Tethys (Gongzha section, Zhang et al., 2019) showing a general similar negative trend supporting a global perturbation of the N cycle. Diagram (C) is a zoom of (B) with TOC restrained to 0 to 10 wt% (greyish area).

Figure 9

Schematic representation of the biogeochemical cycles and hydrological conditions during the deposition of the (A) TH1 and TH3 units and (B) PCE interval within the semi-enclosed Vocontian Basin. Processes labelled as 1 and 2 represent denitrification and anammox, respectively. Representation of the vegetation on land is derived from Heimhofer et al. (2018).

Table 1

Correlation coefficients (r-values, Pearson correlation) of selected trace elements with respect to Al of the n samples analyzed and level of significance of correlations (p-values, expressed in %) associated.

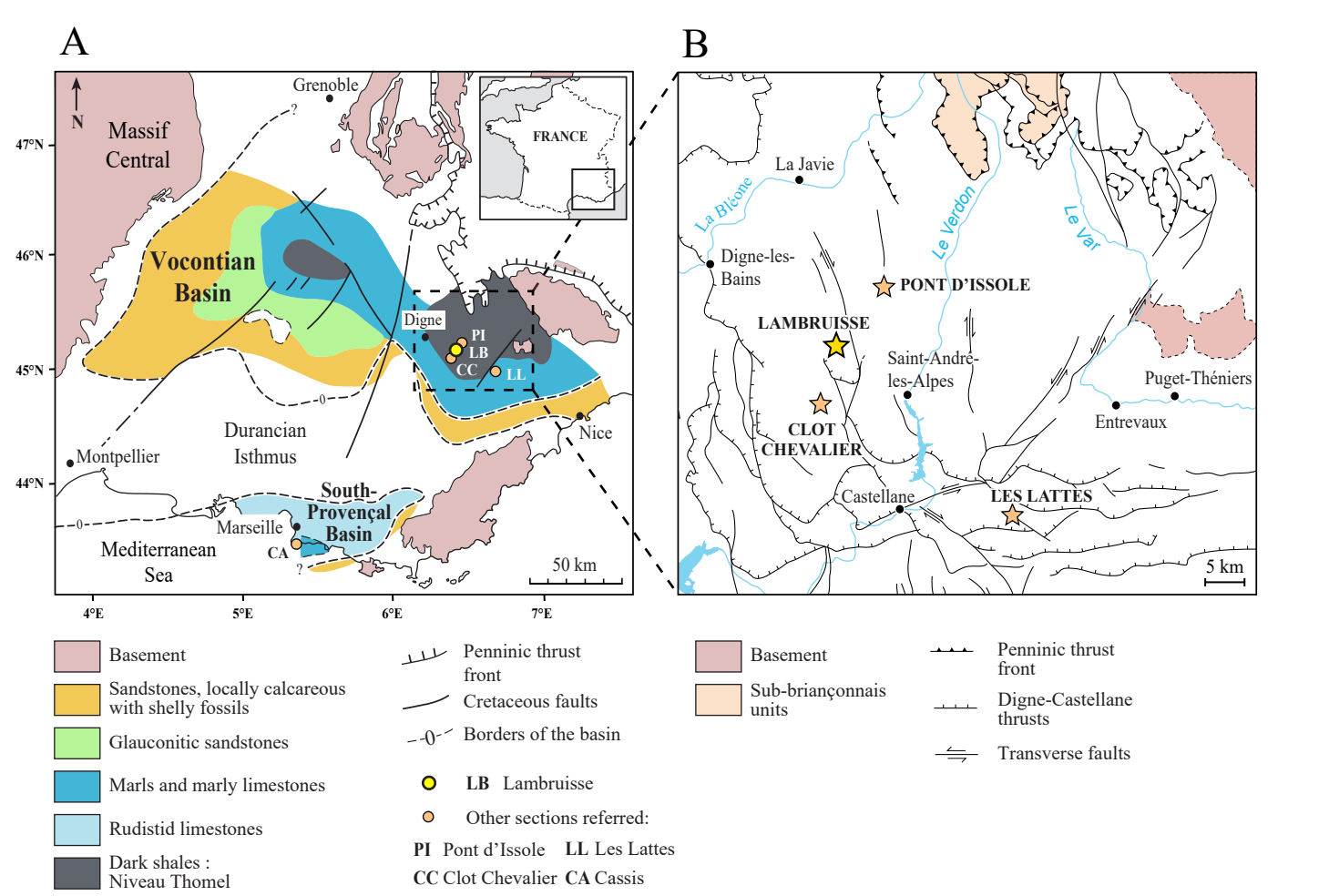
A
B
N
Massif Central
Grenoble
FRANCE
Vocontian Basin
Digne
PI
LB
CC
LL
Durancian Isthmus
Nice
Montpellier
South-Provençal Basin
Marseille
CA
Mediterranean Sea
50 km
47°N
46°N
45°N
44°N
4°E
5°E
6°E
7°E
La Javie
La Bléone
Le Verdon
Le Var
Digne-les-Bains
PONT D'ISSOLE
LAMBRUISSE
Saint-André-les-Alpes
Puget-Théniers
Entrevaux
CLOT CHEVALIER
Castellane
LES LATTES
5 km
Basement
Sandstones, locally calcareous with shelly fossils
Glauconitic sandstones
Marls and marly limestones
Rudistid limestones
Dark shales : Niveau Thomel
Penninic thrust front
Cretaceous faults
Borders of the basin
LB Lambruisse
Other sections referred:
PI Pont d'Issole LL Les Lattes
CC Clot Chevalier CA Cassis
Basement
Sub-briançonnais units
Penninic thrust front
Digne-Castellane thrusts
Transverse faults

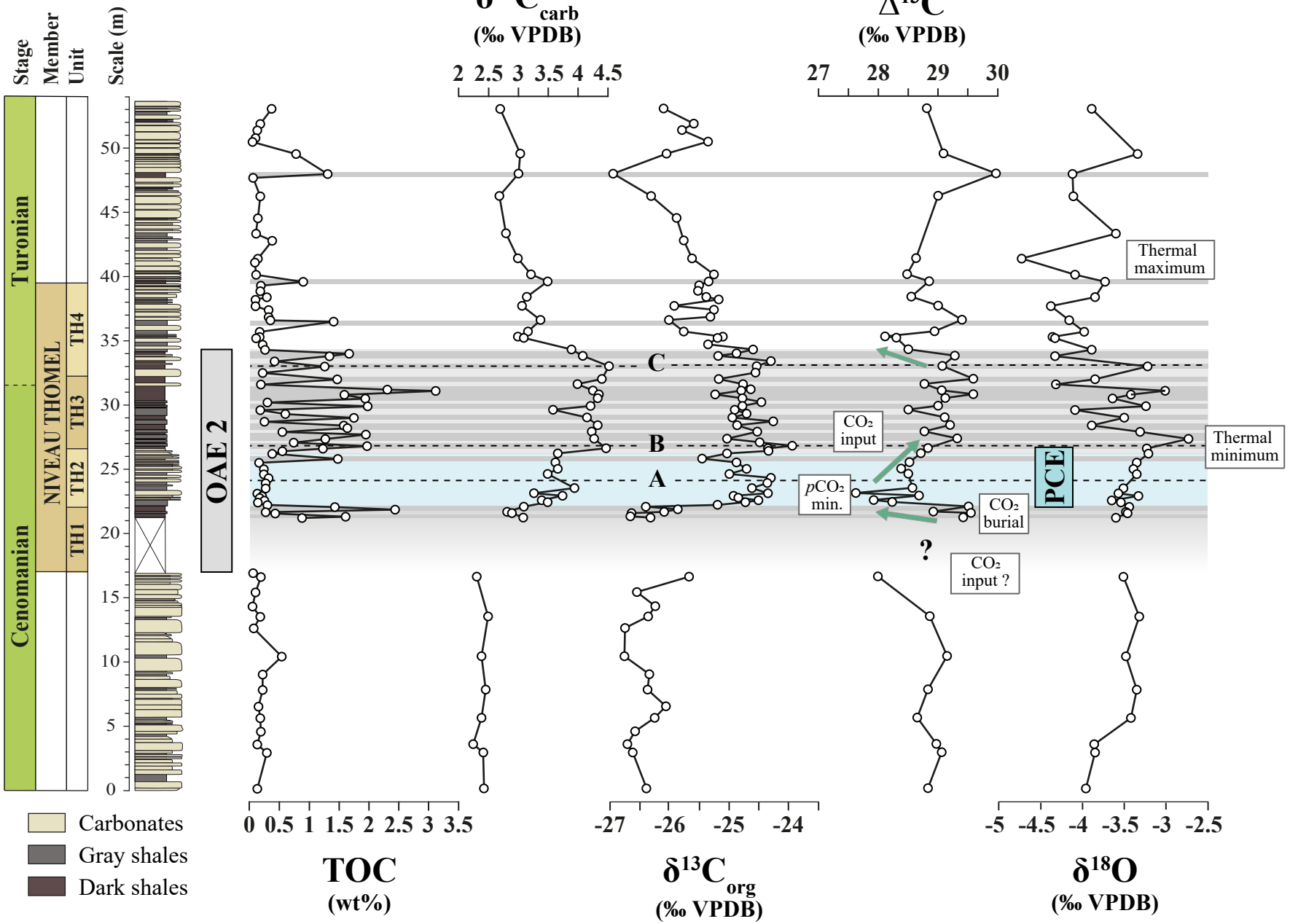
Stage
Member
Unit
Scale (m)
Turonian
Cenomanian
NIVEAU THOMEL
TH4
TH3
TH2
TH1
OAE 2
δ13Ccarb (‰ VPDB)
2 2.5 3 3.5 4 4.5
Δ13C (‰ VPDB)
27 28 29 30
Thermal maximum
C
B
A
CO2 input
pCO2 min.
CO2 burial
PCE
Thermal minimum
?
CO2 input ?
0 0.5 1 1.5 2 2.5 3 3.5
TOC (wt%)
-27 -26 -25 -24
δ13Corg (‰ VPDB)
-5 -4.5 -4 -3.5 -3 -2.5
δ18O (‰ VPDB)
Carbonates
Gray shales
Dark shales

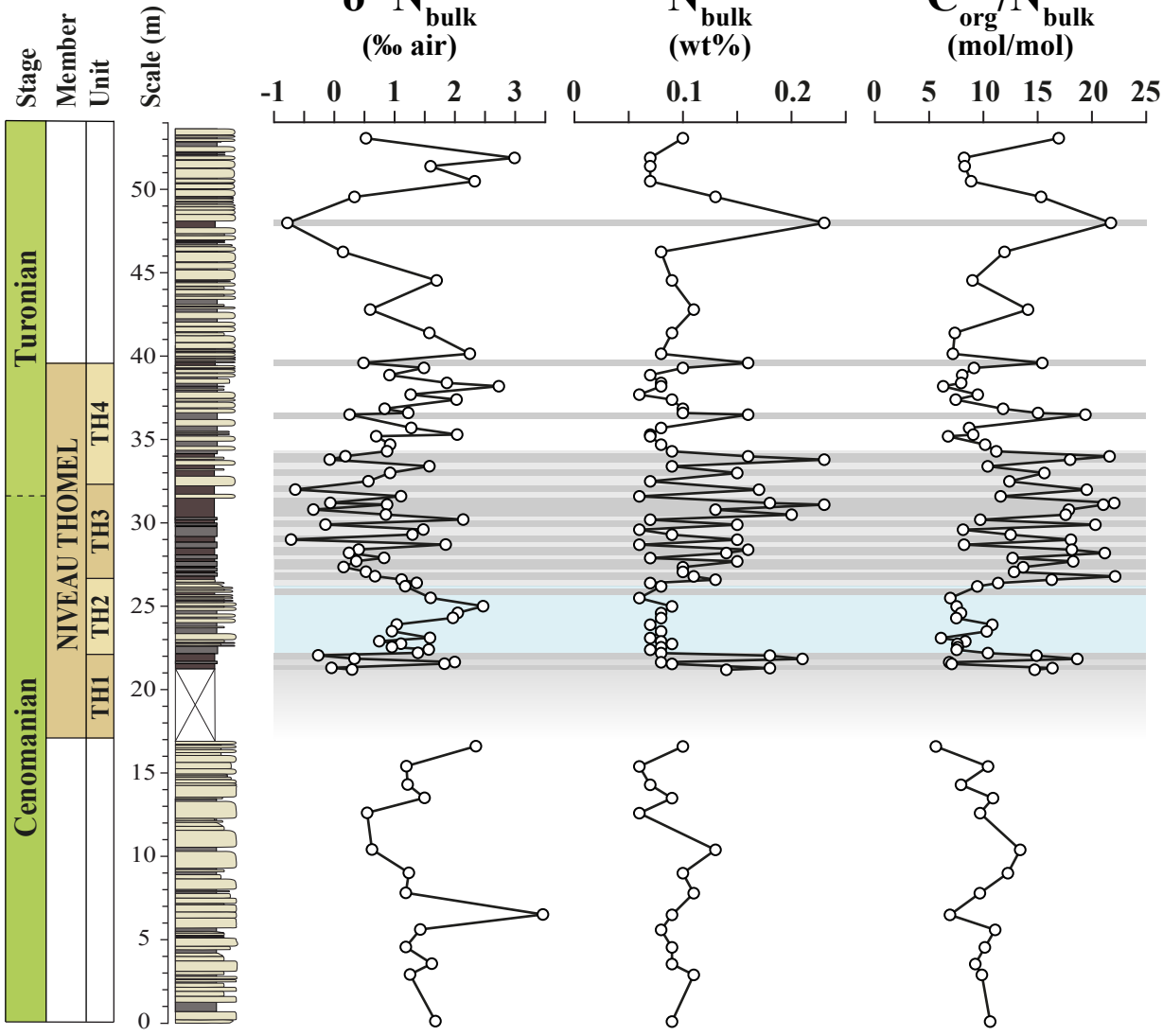
Stage
Member
Unit
Scale (m)
Cenomanian
Turonian
NIVEAU THOMEL
TH1
TH2
TH3
TH4
δ15Nbulk (‰ air)
Nbulk (wt%)
Corg/Nbulk (mol/mol)
-1 0 1 2 3
0 0.1 0.2
0 5 10 15 20 25
0 5 10 15 20 25 30 35 40 45 50

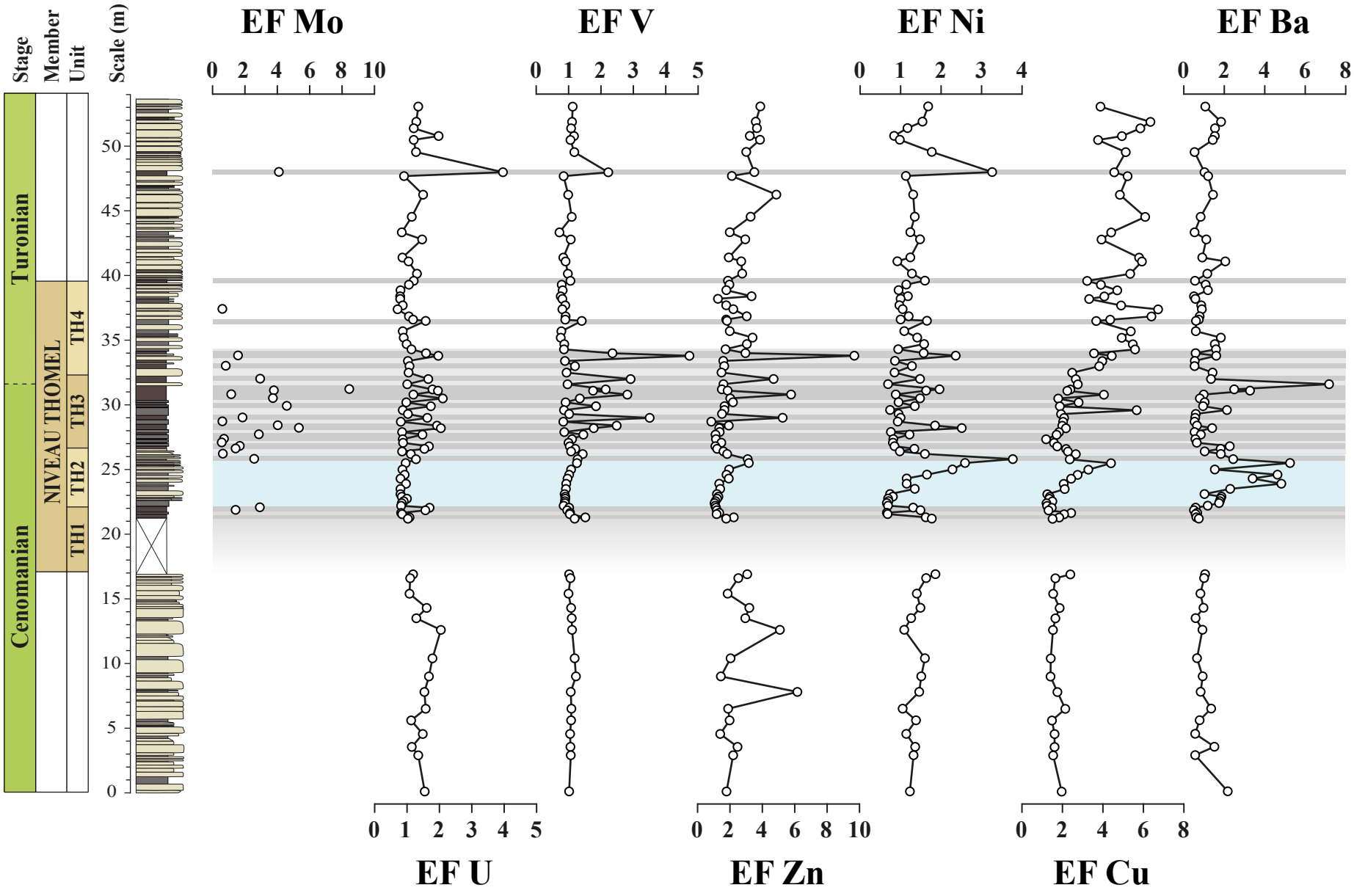
Stage
Member
Unit
Scale (m)
Cenomanian
Turonian
NIVEAU THOMEL
TH1
TH2
TH3
TH4
0
5
10
15
20
25
30
35
40
45
50
EF Mo
0 2 4 6 8 10
EF V
0 1 2 3 4 5
EF Ni
0 1 2 3 4
EF Ba
0 2 4 6 8
EF U
0 1 2 3 4 5
EF Zn
0 2 4 6 8 10
EF Cu
0 2 4 6 8

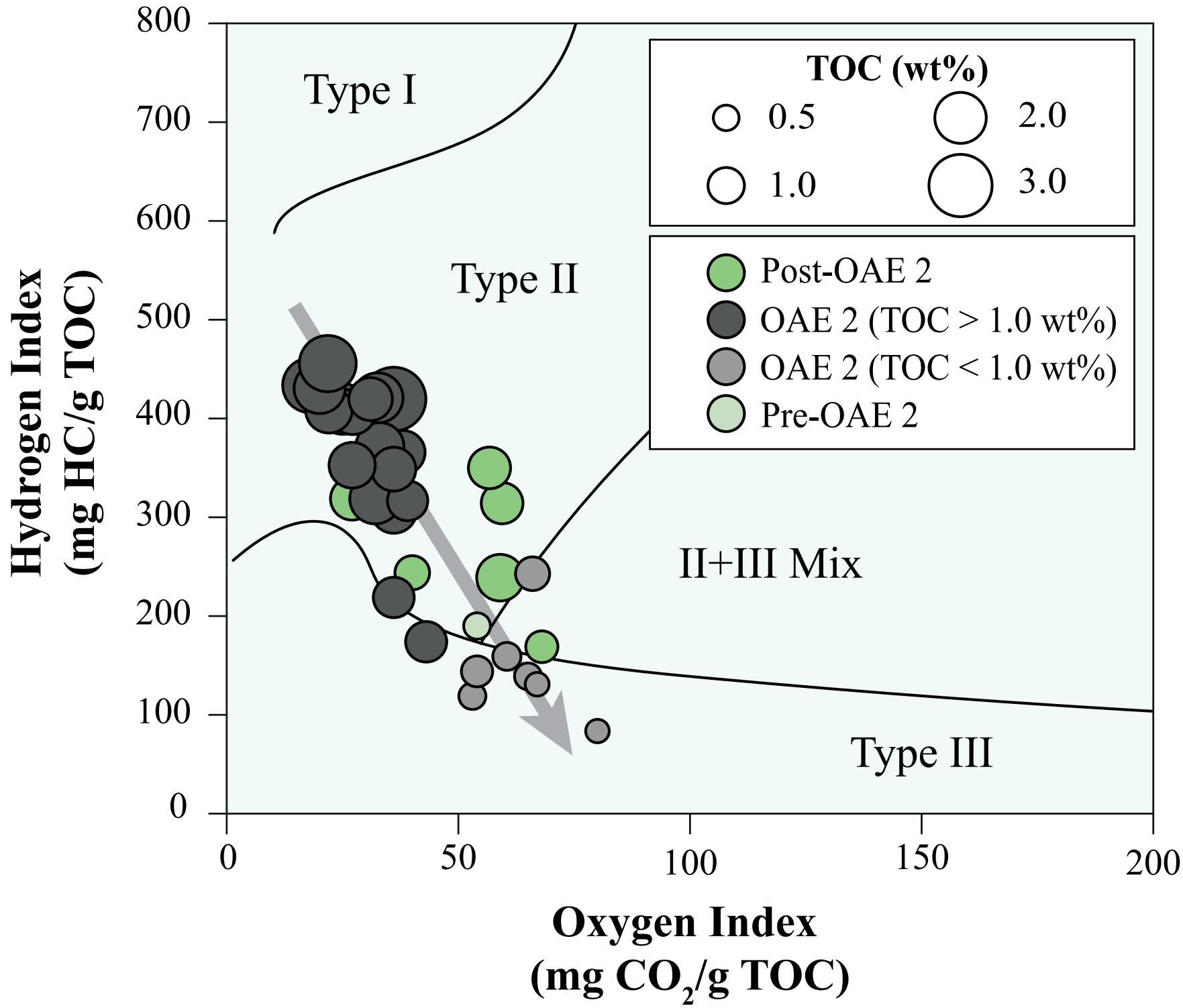
Type I
Type II
II+III Mix
Type III
TOC (wt%)
0.5
1.0
2.0
3.0
Post-OAE 2
OAE 2 (TOC > 1.0 wt%)
OAE 2 (TOC < 1.0 wt%)
Pre-OAE 2
Hydrogen Index
(mg HC/g TOC)
Oxygen Index
(mg CO2/g TOC)
800
700
600
500
400
300
200
100
0
0
50
100
150
200

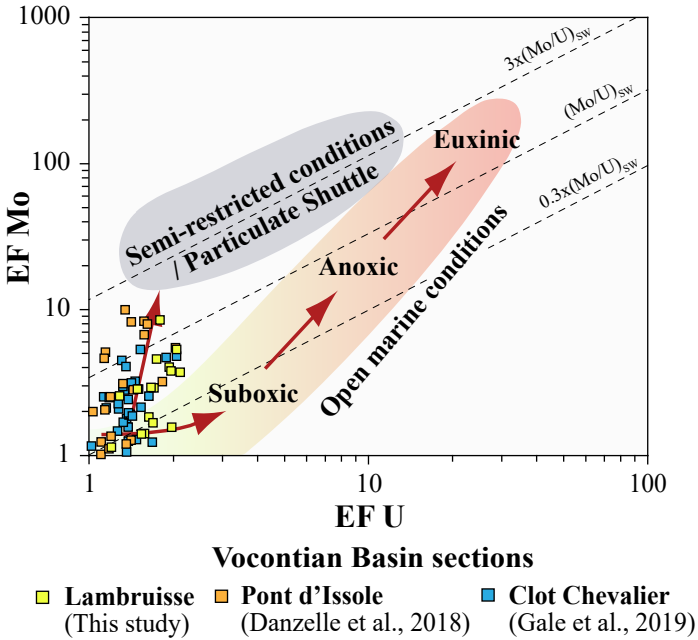
1000
100
10
1
EF Mo
1
10
100
EF U
3x(Mo/U)sw
(Mo/U)sw
0.3x(Mo/U)sw
Euxinic
Anoxic
Suboxic
Semi-restricted conditions
/ Particulate Shuttle
Open marine conditions
Vocontian Basin sections
Lambruisse
(This study)
Pont d'Issole
(Danzelle et al., 2018)
Clot Chevalier
(Gale et al., 2019)

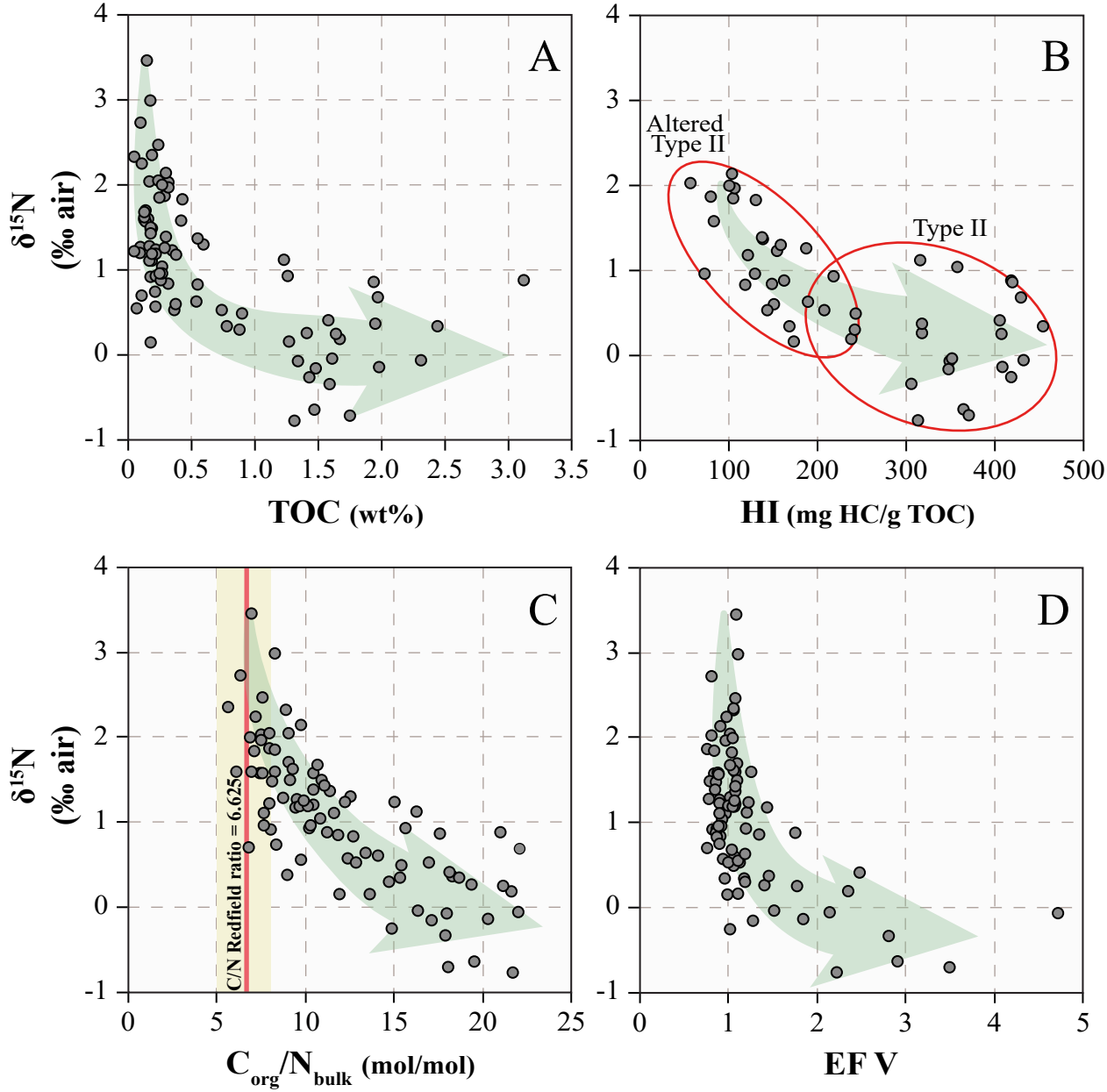
A
B
C
D
δ15N (‰ air)
TOC (wt%)
HI (mg HC/g TOC)
Altered Type II
Type II
C/N Redfield ratio = 6.625
Corg/Nbulk (mol/mol)
EF V

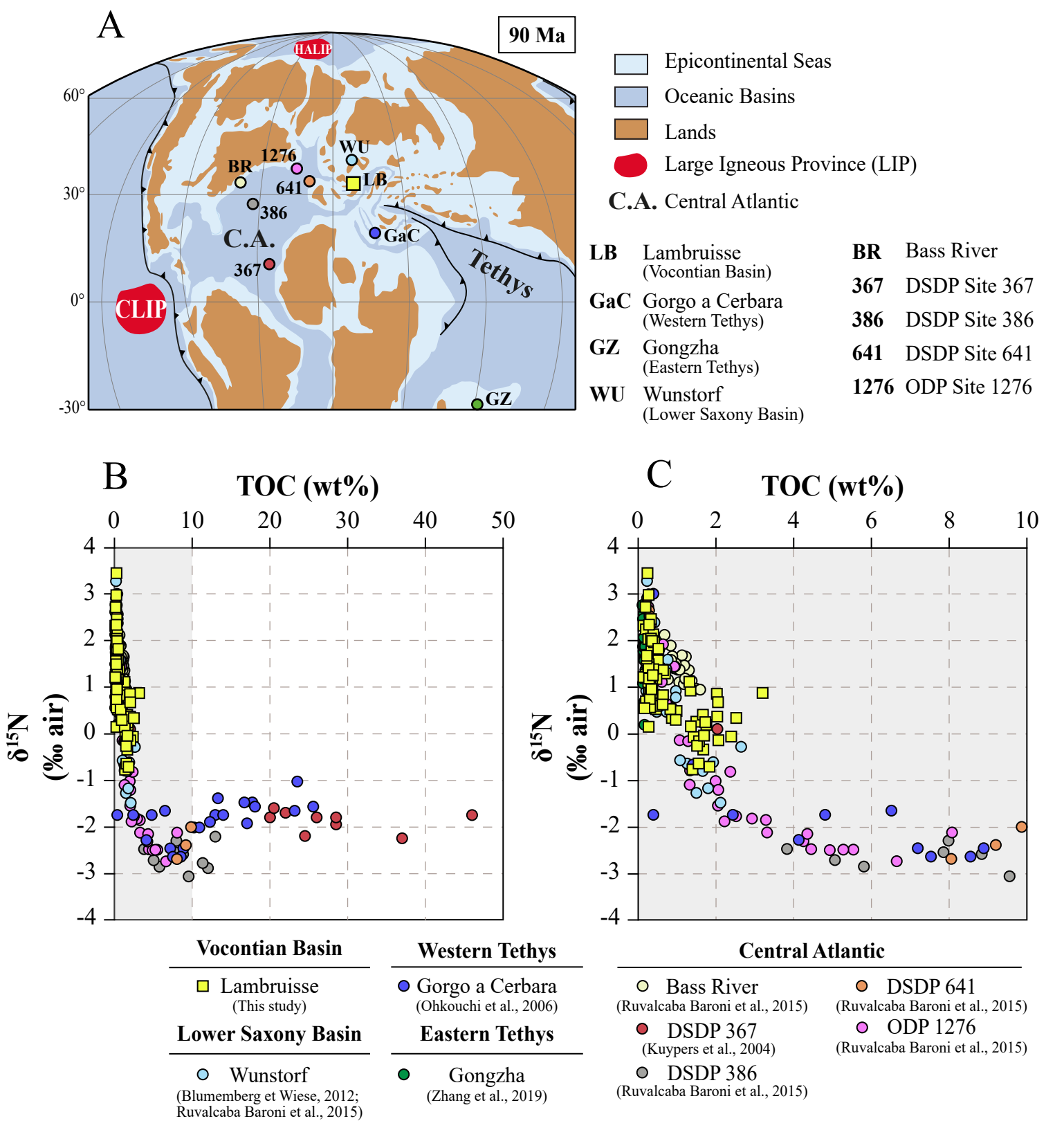
A
90 Ma
HALIP
CLIP
BR
1276
641
386
367
WU
LB
GaC
GZ
C.A.
Tethys
60°
30°
0°
-30°
Epicontinental Seas
Oceanic Basins
Lands
Large Igneous Province (LIP)
C.A. Central Atlantic
LB Lambruisse (Vocontian Basin)
GaC Gorgo a Cerbara (Western Tethys)
GZ Gongzha (Eastern Tethys)
WU Wunstorf (Lower Saxony Basin)
BR Bass River
367 DSDP Site 367
386 DSDP Site 386
641 DSDP Site 641
1276 ODP Site 1276
B
TOC (wt%)
0 10 20 30 40 50
δ15N (‰ air)
4 3 2 1 0 -1 -2 -3 -4
C
TOC (wt%)
0 2 4 6 8 10
δ15N (‰ air)
4 3 2 1 0 -1 -2 -3 -4
Vocontian Basin
Lambruisse (This study)
Western Tethys
Gorgo a Cerbara (Ohkouchi et al., 2006)
Lower Saxony Basin
Wunstorf (Blumemberg et Wiese, 2012; Ruvalcaba Baroni et al., 2015)
Eastern Tethys
Gongzha (Zhang et al., 2019)
Central Atlantic
Bass River (Ruvalcaba Baroni et al., 2015)
DSDP 641 (Ruvalcaba Baroni et al., 2015)
DSDP 367 (Kuypers et al., 2004)
ODP 1276 (Ruvalcaba Baroni et al., 2015)
DSDP 386 (Ruvalcaba Baroni et al., 2015)

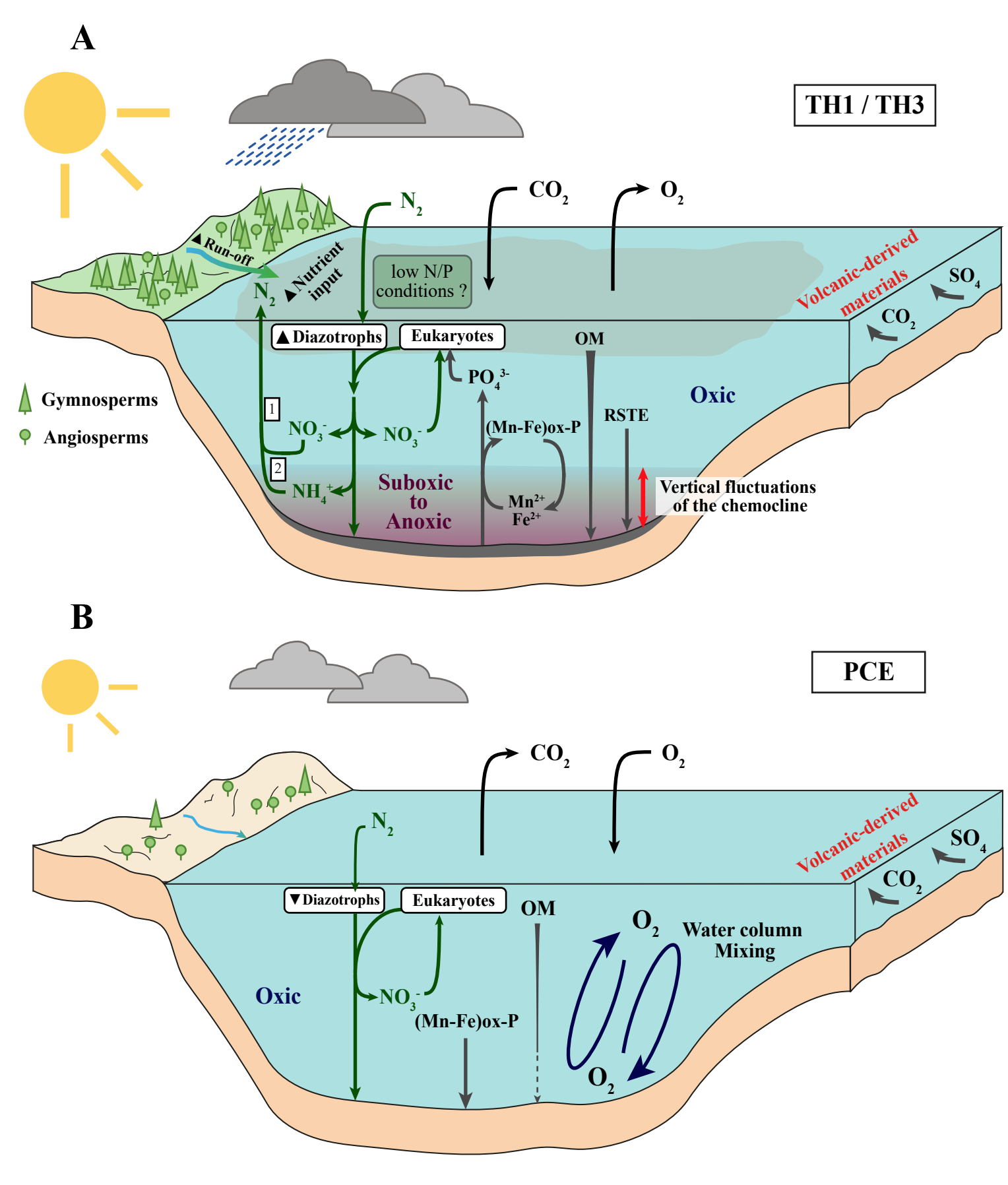
A
TH1 / TH3
N2
CO2
O2
Run-off
Nutrient input
N2
low N/P conditions ?
Volcanic-derived materials
SO4
CO2
Diazotrophs
Eukaryotes
OM
PO4 3-
Oxic
Gymnosperms
Angiosperms
1
NO3-
NO3-
(Mn-Fe)ox-P
RSTE
2
NH4+
Suboxic to Anoxic
Mn2+
Fe2+
Vertical fluctuations of the chemocline
B
PCE
CO2
O2
N2
Volcanic-derived materials
SO4
CO2
Diazotrophs
Eukaryotes
OM
O2
Water column Mixing
Oxic
NO3-
(Mn-Fe)ox-P
O2

Elements	Ba	Cu	Mo	Ni	U	V	Zn	Zr	**TOC**
n	90	90	23	90	90	90	90	90	90
r-value	0.34	0.58	0.10	0.68	0.78	0.71	0.51	0.98	0.60
p-value	<0.005	<0.001	<1	<0.001	<0.001	<0.001	<0.001	<0.001	<0.001